IEEE Access
Multidisciplinary | Rapid Review | Open Access Journal

Received March 15, 2021, accepted April 18, 2021, date of publication April 21, 2021, date of current version May 3, 2021.

Digital Object Identifier 10.1109/ACCESS.2021.3074742

Study and Active Enhancement by Converter Reconfiguration of the Performance in Terms of Stator Copper Loss, Derating Factor and Converter Rating of Multiphase Drives Under Two Open Legs With Different Stator Winding Connections

ALEJANDRO G. YEPES, (Senior Member, IEEE), AND JESÚS DOVAL-GANDOY, (Member, IEEE)
Applied Power Electronics Technology (APET) Research Group, Universidade de Vigo, 36310 Vigo, Spain

Corresponding author: Jesús Doval-Gandoy (jdoval@uvigo.es)

This work was supported in part by the Government of Galicia under Grant ED431F 2020/07, in part by the Ministry of Science, Innovation and Universities under the Ramon y Cajal Grant RYC2018-024407-I, and in part by the Spanish State Research Agency (AEI) under Project PID2019-105612RB-I00/AEI/10.13039/501100011033.

ABSTRACT Multiphase machines offer inherent tolerance to faults such as open converter legs (OCLs), which are especially frequent. Because of this reason, they are particularly attractive for applications where fault tolerance is important, such as offshore wind energy or aerospace, naval and military vehicles. It has been previously shown that, under an OCL, certain stator winding configurations (SWCs) different from star yield smaller stator copper loss (SCL) and larger maximum achievable torque (MAT) than star SWC for the same torque command and machine. This advantage comes just at the expense of a moderate increase in converter rating. However, only the case of single OCL was studied in general. The SCL, MAT and required converter rating for two OCLs are currently unknown for different combinations of phase number, faulted legs and SWCs. Actually, under two OCLs (unlike for one OCL) it may be possible to actively modify the order of the faulted/healthy legs to enhance the performance in these terms, but this possibility has not been studied so far in spite of its potential. This paper addresses the postfault performance of multiphase drives with two OCLs, for various SWCs. The MAT (derating factor), SCL and necessary converter rating are assessed in numerous possible scenarios. The most convenient alternatives are established. Most importantly, in view of the conclusions of this analysis, a novel method is proposed to improve substantially the MAT and SCL by actively altering the connections between the converter and machine terminals. Experimental results with six-phase and twelve-phase setups are provided.

INDEX TERMS Derating factors (DFs), fault-tolerant, five-phase, minimum copper losses, multiphase drives, six-phase, stator winding configuration (SWC), twelve-phase, symmetrical, variable speed drives.

ACRONYMS

DF	Derating factor.
FRMLS	Full-range minimum-loss strategy.
MAT	Maximum achievable torque.
OCL	Open converter leg.
SCL	Stator copper loss.
SWC	Stator winding configuration.
VSD	Vector space decomposition.

VARIABLES

λ Denotes an SWC based on series connection of each pair of phases with $\lambda\gamma$ spatial step between them.

The associate editor coordinating the review of this manuscript and approving it for publication was Feifei Bu.

$\eta_{\lambda,1}$	Metric of SCL of the λ SWC compared with $\lambda = 1$.
$\eta_{\mu,1}$	Metric of SCL of the μ case compared with $\mu = 1$.
$\eta_{\mu,2}$	Metric of SCL of the μ case compared with $\mu = 2$.
γ	Spatial step between neighboring stator phases, $= 2\pi/n$.
i	Stator current.
$\lvert i_{\alpha\beta_1} \rvert$	Modulus of α_1-β_1 (flux/torque-producing) current, $= \sqrt{i_{\alpha_1}^2 + i_{\beta_1}^2} = \sqrt{i_{\mathrm{d}}^2 + i_{\mathrm{q}}^2}$.
i_{d}	d-axis current, aligned with rotor flux in α_1-β_1 plane.
i_{q}	q-axis current, orthogonal to rotor flux in α_1-β_1 plane.
i^{rc}	Rated phase-current peak.
μ	Spatial step between stator phases affected by OCLs, as a multiple of γ.
n	Number of phases.

I. INTRODUCTION

Multiphase drives present various benefits in comparison with three-phase ones [1]–[5]. Among these advantages, the superior fault-tolerance capability frequently receives special attention [1]–[46]. In fact, multiphase drives are considered of great interest for applications where tolerance to faults is important or crucial, such as standalone/offshore wind/hydro energy conversion systems, aircraft and military vehicles (even low-power ones) [5]. The majority of the faults in electric drives are related to the power electronics [5], [23], and the case of OCLs is of particular relevance [8], [12]–[14]. The latter can be the result, e.g., of an open switch or of remedial actions applied by fuses or circuit breakers (e.g., in case of short-circuit switch faults) [9], [28], [29], [32], [33], [47], [48].

To drive an n-phase machine, a converter of, e.g., n, $n+1$ or $2n$ legs can be adopted [49]. More than n legs can be interesting in some cases for obtaining even more degrees of freedom (e.g., for special machines that need 0^+ zero-sequence current in healthy conditions) [49] at the expense of extra size and cost. Nevertheless, n legs is normally sufficient and is arguably a very common option in multiphase fault-tolerant drives [1], [2], [6]–[9], [12]–[22], [24]–[40]. Thus, n-leg converters are considered throughout this paper.

In an n-phase machine with symmetrical winding arrangement (consecutive phases displaced by $\gamma = 2\pi/n$ [2], [25]), there are several possible SWCs, whose number increases with n [8], [12]–[15], [21], [22], [49]–[53]. A general way to denote each of these SWCs is by means of the variable λ [8]. Namely, the λ SWC results by connecting in series (ignoring the converter) every pair of phases such that the spatial step between them spans an angle $\lambda\gamma$ (i.e., λ phases) in the stator. The star SWC is represented by $\lambda = 0$. For instance, the SWCs for $n = 6$ are illustrated in Fig. 1 [8].

The most common SWC is star [49], [50], followed by $\lambda = 1$ [8], [12]–[15], [21], [22], [50], i.e., connecting each phase in series with the one that is next in the stator physical disposition. For $n = 5$, Abdel-Khalik *et al.* [12]–[14] have

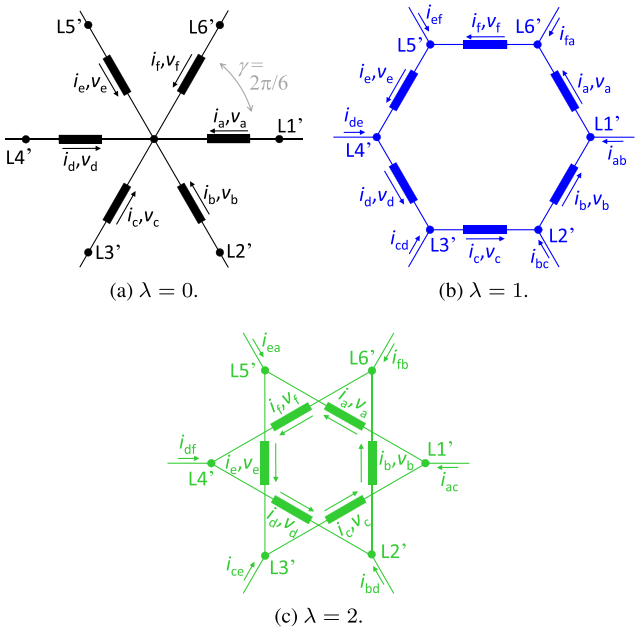

FIGURE 1. SWCs in a six-phase machine [8].

shown that, under an OCL, the $\lambda = 1$ SWC yields smaller SCL for the same torque command and machine, as well as larger MAT, than the star SWC. This can be achieved at the only cost of setting a slightly greater converter current rating. Recently, it was proved in [8] that $\lambda = 1$ is the best SWC regarding MAT and SCL for $n > 5$ as well, and that for $n > 5$ the amount of improvement provided by $\lambda = 1$ increases drastically with respect to $n = 5$. It was also concluded that, for roughly $n > 10$, the $\lambda = 1$ SWC requires a very large voltage rating of the converter, compared with star; but $\lambda = 2$ can be instead adopted for $n > 10$, with reasonable converter rating and with nearly as good MAT and SCL performance as $\lambda = 1$. However, only the scenario of a single OCL was taken into account [8]. Nevertheless, often two phases/legs instead of one become faulty, and hence such situation should also be considered [7], [9], [17], [20], [21], [26], [30], [31], [34], [35], [37], [41].

The values of MAT (or equivalently, DF), SCL and required converter rating for a given scenario (faulted leg/s, SWC and number of phases) are useful *per se* as indicators of the goodness of the postfault performance [6], [8], [9], [25]–[27], [37]. They have been assessed in [6], [9], [25]–[27], [37] for asymmetrical/symmetrical six-phase machines with star SWC and one or several OCLs, and in [8] for symmetrical n-phase machines of various n and SWCs with a single OCL. However, the SCL, MAT and necessary converter rating for symmetrical multiphase machines with different phase numbers, SWCs and two OCLs are yet to be determined. Furthermore, under two OCLs (unlike for one OCL), it may be possible to actively modify the disposition of the converter faulted/healthy legs with respect to the stator terminals in order to enhance the postfault performance in terms of SCL and MAT; but

this possibility has not been tackled so far, in spite of its potential. In this regard, establishing the performance of each scenario/configuration is also necessary in order to be able to set the disposition of the converter faulted/healthy legs for the best behavior after two OCL faults occur.

This paper addresses, in the first place, the postfault performance of symmetrical multiphase machines under two OCLs for three SWCs: $\lambda = 0, 1, 2$, which are the most convenient for healthy drive or single OCL [8]. The MAT (or equivalently, DF), SCL and needed converter rating under such conditions are assessed and compared, in multiple scenarios. It is shown that the performance is highly dependent on the specific pair of phases affected by OCLs. Accordingly, a novel technique is proposed to substantially improve the MAT and SCL by using relays or switches to conveniently modify the connections between the converter legs and machine stator terminals, without having to stop or disassemble the drive. In contrast to the converter reconfiguration proposed in [37] for star SWC, here it is not necessary to have accessible dc-link midpoint or to oversize the dc-link capacitors. Some considerations about more than two OCLs are also given through the paper. Experimental results with two setups, of six and twelve phases, are provided. In the preliminary version [54], only the particular case of $n = 6$ with $\lambda = 0, 1$ SWCs was addressed (here, $n =$ 5-15 with $\lambda = 0, 1, 2$), and the transient behavior was not tested (here, experimentally).

The paper is organized as follows. In Section II, some fundamentals are briefly reviewed. The performance obtained with two OCLs is studied in Sections III, IV and V in terms of DF, SCL and converter rating, respectively. In Section VI, the method for improvement of postfault performance under two OCLs is proposed. Experimental results are presented in Section VII. Finally, Section VIII concludes the work.

II. BACKGROUND

A. VECTOR SPACE DECOMPOSITION

The model of a symmetrical n-phase machine can be decomposed by using the VSD into $\lfloor n/2 \rfloor + 1$ subspaces, for any SWC [2], [8]. These subspaces consist of $P = \lceil n/2 \rceil - 1$ planes (α_1-β_1, α_2-β_2, etc.) and one or two zero-sequence axes (0^+ and 0^-) for odd or even n, respectively. An electrical variable u (voltage v or current i) given in stator per-phase values can be transformed as follows [2], [8]:

$$\begin{aligned}&\left[u_{\alpha_1}\ u_{\beta_1}\ u_{\alpha_2}\ u_{\beta_2}\ \ldots\ u_{\alpha_P}\ u_{\beta_P}\ u_{0^+}\ u_{0^-}\right]^{\mathrm{T}}\\&\quad = H\left[u_{\mathrm{a}}\ u_{\mathrm{b}}\ \ldots\ u_n\right]^{\mathrm{T}};\end{aligned} \tag{1}$$

$$H = \frac{2}{n}\begin{bmatrix} 1 & \cos(\gamma) & \cos(2\gamma) & \ldots & \cos(n'\gamma) \\ 0 & \sin(\gamma) & \sin(2\gamma) & \ldots & \sin(n'\gamma) \\ 1 & \cos(2\gamma) & \cos(4\gamma) & \ldots & \cos(2n'\gamma) \\ 0 & \sin(2\gamma) & \sin(4\gamma) & \ldots & \sin(2n'\gamma) \\ \vdots & \vdots & \vdots & \ddots & \vdots \\ 1 & \cos(n'\gamma) & \cos(2n'\gamma) & \ldots & \cos\left[(n')^2\gamma\right] \\ 0 & \sin(n'\gamma) & \sin(2n'\gamma) & \ldots & \sin\left[(n')^2\gamma\right] \\ 1/2 & 1/2 & 1/2 & \ldots & 1/2 \\ 1/2 & -1/2 & 1/2 & \ldots & -1/2 \end{bmatrix} \tag{2}$$

where $\gamma = 2\pi/n$ and $n' = n - 1$. If the windings are sinusoidally distributed, the u_{α_1} and u_{β_1} variables are related to flux and torque, and the rest (u_{0^+}, u_{0^-}, u_{α_2}, u_{β_2}, etc.), only to losses [1], [2]. The u_{0^-} component only exists if n is even; otherwise, it is necessary to omit u_{0^-} in (1) and the last row of (2). On the other hand, although the variable u_{0^+} exists regardless of n, normally i_{0^+} is zero or negligible [8]. The latter is because for $\lambda = 0$ a single neutral point is considered (it gives better postfault performance [6], [9], [33]), machine space harmonics [2], [11], [55] are neglected, and it is assumed that i_{0^+} is not necessary for healthy operation (unlike, e.g, in some special machines [49]). Asymmetrical winding arrangements are not included in the analysis to avoid excessive length and because their postfault performance is inferior to symmetrical ones [9], [25].

B. DERATING FACTOR AND MAXIMUM ACHIEVABLE TORQUE

The maximum torque that can be attained (i.e., the MAT) under OCLs is lower than in healthy conditions, because the machine rated current rms $i^{\mathrm{rc}}/\sqrt{2}$ (rc stands for rated conditions) should not be surpassed in any of the remaining phases.[1] This MAT reduction (derating) is a relevant figure of merit to evaluate postfault performance [6], [9], [25], [37]. In particular, the DF is the maximum achievable (without $i > i^{\mathrm{rc}}$ in any stator phase) value of the α_1-β_1 (or d-q, in synchronous frame) current modulus

$$\left|i_{\alpha\beta_1}\right| = \sqrt{i_{\alpha_1}^2 + i_{\beta_1}^2} = \sqrt{i_{\mathrm{d}}^2 + i_{\mathrm{q}}^2} \tag{3}$$

normalized with respect to rated healthy operation (from now on, simply "normalized"), i.e., divided by $|i_{\alpha\beta_1}^{\mathrm{rc}}| = i^{\mathrm{rc}}$ [8]–[11]. Since the machine torque depends on $|i_{\alpha\beta_1}|$,[2] the DF is closely related to the MAT; for certain machine, higher DF also implies higher MAT [8]–[11]. Nevertheless, the DF is more general than the MAT in the sense that it does not depend on the machine type (induction, permanent-magnet, etc.), machine parameters, rated power, speed, how $|i_{\alpha\beta_1}|$ is distributed between i_{d} and i_{q}, etc. [8]–[11]. Note that, although the DF is defined as a $\left|i_{\alpha\beta_1}\right|$ value, the current constraints imposed by the SWC and OCLs normally imply that under fault there is also current in the other subspaces depending on $\left|i_{\alpha\beta_1}\right|$, and these components indirectly affect whether the $i \leq i^{\mathrm{rc}}$ condition is satisfied in all phases or not for given $\left|i_{\alpha\beta_1}\right|$ (and hence, the DF value).

It is assumed that, to avoid exceeding the current and voltage ratings of the converter when there are OCLs and the machine is working at the MAT, the converter ratings are suitably adjusted during the design stage [8], [47], instead of setting the converter ratings just based on healthy operation. Otherwise, to avoid converter damage, the MAT of the drive

[1] By using the machine thermal model, it is possible to set higher phase current than rated [43]–[45], but this requires knowledge of such model and it implies extra converter current overrating and additional complexity.

[2] Further explanation about the relation between $|i_{\alpha\beta_1}|$ and torque can be found, e.g., in Sections 2.2 and 2.3 of [8].

would have to be further reduced (not considered here) in certain fault scenarios.

C. STRATEGY FOR CURRENT-REFERENCE OPTIMIZATION

Although under fault the α_1-β_1 current reference is set as in healthy conditions and the current in the other subspaces depends on the former due to current constraints, there are still degrees of freedom to set the latter according to additional design criteria. Most of the existing methods for generation of current references in postfault condition are based on fixed coefficients that do not depend on the flux/torque requirement, and can be classified into two groups: minimum-loss and maximum-torque strategies [5], [6], [9], [24], [25], [27]. The former ensures minimum SCL, but the potential MAT (or the maximum $|i_{\alpha\beta_1}|$) for a given fault scenario cannot be reached ($i > i^{rc}$ would occur). On the contrary, the maximum-torque strategy is able to produce the MAT without overcurrent, but it does not optimize SCL. A technique to minimize SCL for each torque (or $|i_{\alpha\beta_1}|$) command, while providing a torque operation range up to the postfault MAT, was proposed in [25]. It was called FRMLS. Basically, it is based on setting the current references in the flux/torque-producing plane (α_1-β_1) as in healthy machine, and computing the references in other subspaces (0^-, α_2-β_2, α_3-β_3, etc.) so as to minimize SCL under the system restrictions for each possible torque command (or $|i_{\alpha\beta_1}|$ value). Coefficients varying as a function of $|i_{\alpha\beta_1}|$ are employed for this purpose during the drive operation. Ideally, iron loss only depends on the α_1-β_1 current reference (through the α_1-β_1 frequency and flux [56]), not on the other subspace currents defined by the postfault strategy, and hence it does not need to be accounted for in the latter [26]. It was also proved that this approach yields optimum converter loss [27]. Later, the FRMLS was applied to asymmetrical six-phase machines with two OCLs [26], [37] and to n-phase machines with one OCL and different SWCs [8] by adding suitable current constraints to the optimization problem. Voltage restrictions were also included in the context of machines with star SWC in field-weakening operation and with isolated/connected neutral points [16]. Simplified implementation was addressed in [17]. The effect of rotor and core loss were addressed in [42] for a five-phase machine with significant space harmonics.

For this paper, to apply the FRMLS to n-phase machines with several SWCs and two OCLs, the version of the method described in [8] for single OCL is adopted, and then an additional restriction is included for the second OCL: the corresponding line current supplied by the converter is imposed to be zero. The FRMLS is used in this manner throughout this work to obtain the SCL, DF (or MAT) and necessary converter rating in various scenarios. Namely, the SCL and converter rating are computed based on the optimum currents obtained by the FRMLS for each $|i_{\alpha\beta_1}|$ and fault/SWC scenario, and the DF for given scenario is the maximum $|i_{\alpha\beta_1}|$ such that the FRMLS has solution [8]. For the sake of generality and simplicity, the stator-impedance voltage drop is neglected in comparison with the back-electromotive force at high speeds. It should also be emphasized that the FRMLS is not claimed to be a contribution of this paper.

III. ANALYSIS OF DF FOR TWO OCLs

The converter legs/lines are denoted L1, L2, …, Ln. The respective stator terminals are L1', L2', …, Ln', as shown in Fig. 1. This correspondence between converter lines and stator terminals holds unless a postfault reconfiguration is deliberately applied (addressed later). For star, the order of stator terminals is such that L1', L2', …correspond to stator phases a, b, …, respectively. For $\lambda = 1$ SWC, L1' is connected to phases a and b, L2' to phases b and c, etc. For $\lambda = 2$ SWC, L1' is connected to phases a and c, L2' to phases b and d, etc.

For single OCL, the postfault performance does not depend on the particular line with OCL [8]. Conversely, for two OCLs, various fault scenarios, with different performance, should be separately studied for given n and SWC. For this purpose, in this paper the variable μ is defined. Namely, when there are two OCLs, μ indicates the stator terminal affected by one OCL (i.e., with no current through its respective line) in relative terms with respect to the other stator terminal also affected by OCL. For instance, if $\mu = 1$ two consecutive stator terminals (e.g., L1' and L2') have zero line current, if $\mu = 2$ there is a healthy one between two (e.g., L1' and L3') without line current, etc. Due to symmetry, all the possible combinations of two faulty lines are covered (regarding performance) by sweeping μ from 1 to $\lfloor n/2 \rfloor$.

For all the scenarios with two OCLs and with n between five and fifteen, the DF (defined in Section II-B) is calculated by a procedure analogous to that applied in [8, Fig. 2] for single OCL. Although some of these phase numbers (e.g., 8, 10 and 14) are unusual in practice, they are also considered here for the sake of generality and for facilitating the assessment of the overall trends. The resulting DFs are depicted in Fig. 2. The dashed, solid and dotted lines correspond to the $\lambda = 0$, $\lambda = 1$ and $\lambda = 2$ SWCs, respectively. SWCs of greater λ are discarded, since it was shown in [8] that they yield larger line current for healthy or faulty operation, as well as worse DF and SCL for one OCL. Each color in Fig. 2 is associated to a μ value. Such μ numbers are indicated at the beginning of the corresponding curves, with the same color; in addition, these initial points are also marked by relatively big circles. The line for $\lambda = 2$ and $\mu = 3$ begins at $n = 6$ with a DF of zero. Note that all the plots continue until the highest n under consideration, $n = 15$.

A. ANALYSIS FOR $\lambda = 0$ AND $\lambda = 1$

From Fig. 2, three general deductions can be drawn concerning the $\lambda = 0$ (star) and $\lambda = 1$ SWCs.

1) For each μ, the DF with $\lambda = 1$ is substantially larger than with $\lambda = 0$.
2) The DF difference between the possible μ values vastly decreases with increasing n (except for very low n).

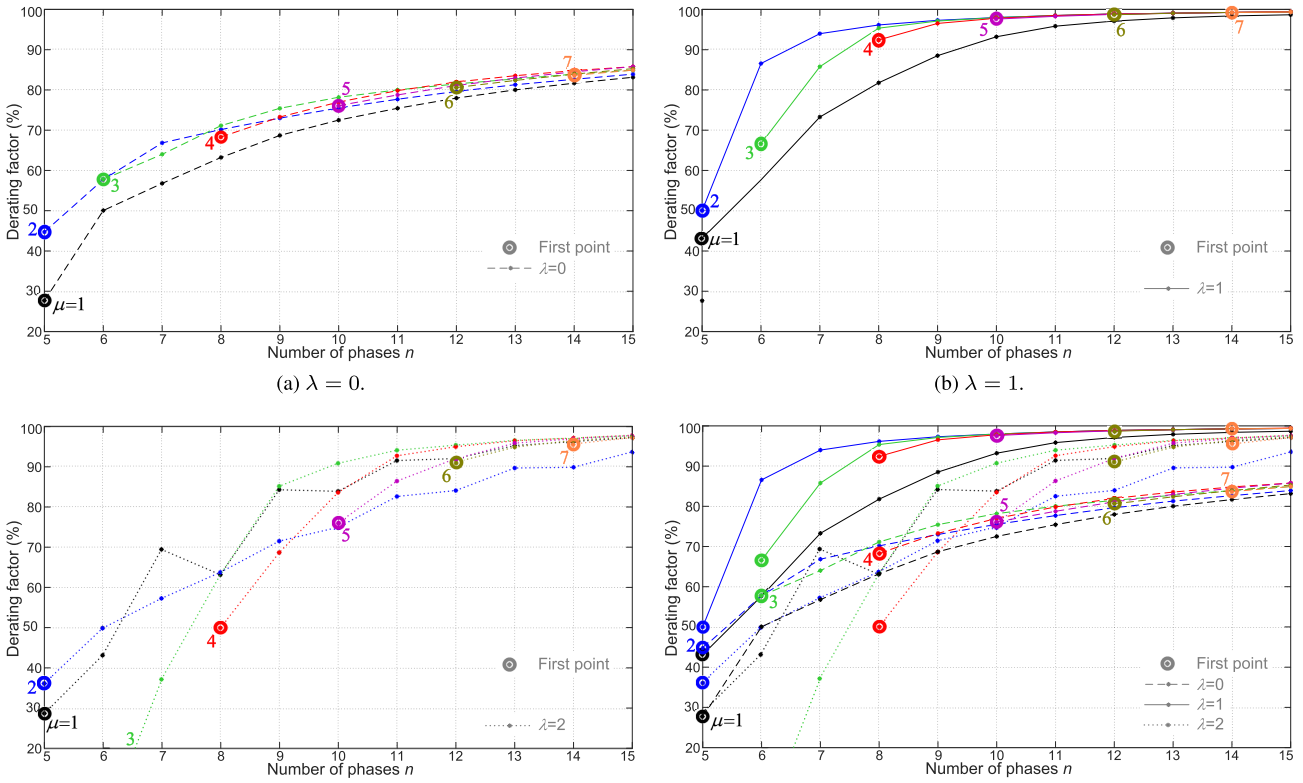

(a) $\lambda = 0$. (b) $\lambda = 1$.

(c) $\lambda = 2$. (d) $\lambda = 0$, $\lambda = 1$ and $\lambda = 2$ together (for comparison).

FIGURE 2. DF of the $\lambda = 0$ (dashed), $\lambda = 1$ (solid) and $\lambda = 2$ (dotted) SWCs for different μ (black for $\mu = 1$, blue for $\mu = 2$, green for $\mu = 3$, etc.).

3) In most cases where the DF varies with μ considerably (low n), $\mu = 1$ and $\mu = 2$ are the least and the most convenient μ scenarios, respectively.

This is further studied next using various comparative figures. These three observations are referred to in the following paragraphs as conclusions 1), 2) and 3).

The solid curves in Fig. 3 represent the difference in DF between $\lambda = 1$ and $\lambda = 0$ (the former minus the latter), for each μ. Such difference is always positive, and significant for most n, confirming conclusion 1). The DF improvement provided by $\lambda = 1$ in comparison with $\lambda = 0$ for two OCLs is, in many scenarios, even larger than that for single OCL [8, Fig. 3]. For instance, for two OCLs, the largest increase is 28.9% ($n = 6$ with $\mu = 2$); for single OCL, it is 12.7% ($n = 6$) [8]. Note that, through this paper, DF differences are expressed as percentages because the DF values subtracted are already percentages (of rated and healthy conditions), not because the DF differences are computed (they are not) in relative terms with respect to any of the two scenarios compared each time.

The result of subtracting the $\mu = 1$ DF from the DF of each μ is represented in Fig. 4(a) and (b) for $\lambda = 0$ and $\lambda = 1$, respectively. The reduction in these curves as n rises further verifies conclusion 2). Conclusion 3) is corroborated by the facts that such DF difference is always positive and that, for most n, it is greater with $\mu = 2$ than with any other μ. Actually, in Fig. 4, $\mu = 2$ exhibits peaks of 17.1% for $\lambda = 0$ ($n = 5$) and 28.9% for $\lambda = 1$ ($n = 6$). For $n \geq 8$ with star, $\mu = 3$ permits higher DF than $\mu = 2$, but then the deviation between them is also less significant, smaller than 3% [see Fig. 4(a)].

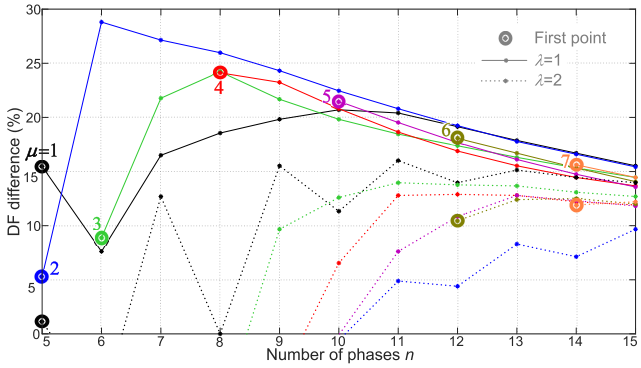

FIGURE 3. DF difference between $\lambda = 1$ and $\lambda = 0$ SWCs (solid) and between $\lambda = 2$ and $\lambda = 0$ SWCs (dotted), for each μ.

B. ANALYSIS FOR $\lambda = 2$

The $\lambda = 2$ SWC is recommendable for $n > 10$ in case of a single OCL, because then it provides nearly as good DF and SCL as $\lambda = 1$, but with not as large converter voltage rating [8]. Concerning DF for two OCLs, it can be seen in Figs. 2 and 3 that for $n > 10$ the DF of $\lambda = 2$ is higher and lower than that of $\lambda = 0$ and $\lambda = 1$, respectively.

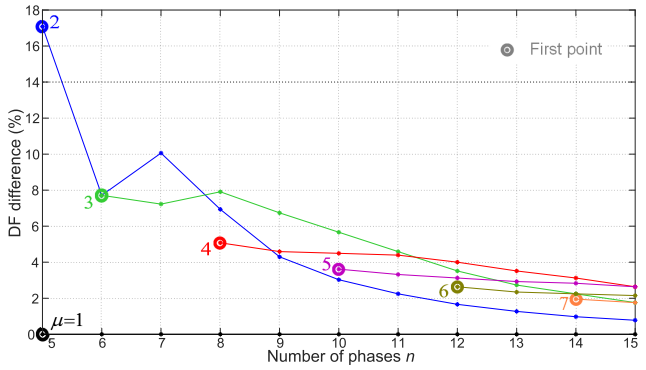

(a) Between each μ and $\mu = 1$ for $\lambda = 0$ SWC.

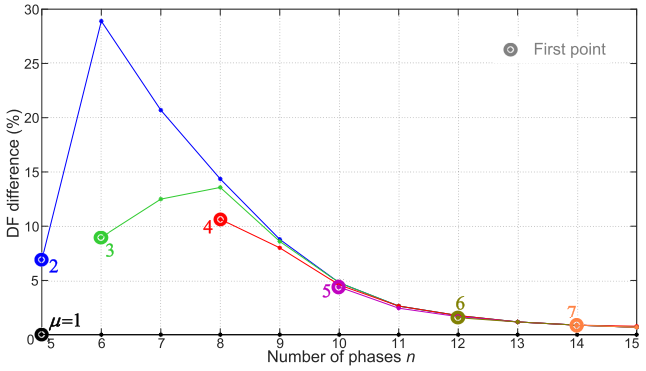

(b) Between each μ and $\mu = 1$ for $\lambda = 1$ SWC.

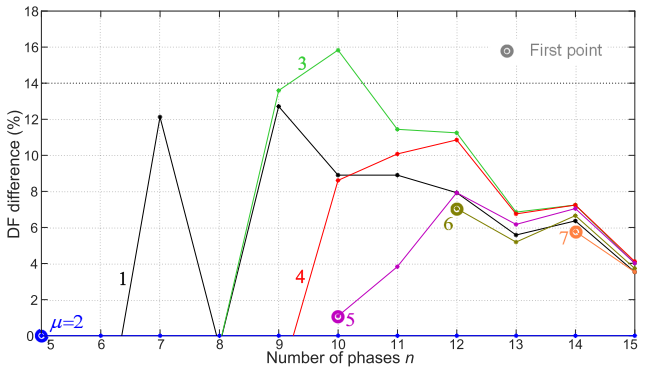

(c) Between each μ and $\mu = 2$ for $\lambda = 2$ SWC.

FIGURE 4. **DF difference between different μ, for each SWC.**

Furthermore, in this n range, the $\lambda = 2$ DF is closer to the $\lambda = 1$ DF than to the $\lambda = 0$ DF for most μ, and this is accentuated as n rises. Accordingly, due to this similarity between the $\lambda = 1$ and $\lambda = 2$ DFs, it can also be stated that (at least for high n) the advantage of $\lambda = 2$ over $\lambda = 0$ in DF for two OCLs is often larger than for single OCL, as with $\lambda = 1$. For instance, for $n = 15$ the DF increase provided by $\lambda = 2$ over $\lambda = 0$ for one OCL is 6.2% in case of one OCL [8], but it is 9.7%-14.0% for two OCLs (see Fig. 3).

From Fig. 2, for each n value greater than 10, the highest and lowest DF is obtained for $\mu = 3$ and $\mu = 2$, respectively, which differs from the behavior assessed earlier for $\lambda = 0$ and $\lambda = 1$. This statement about the $\mu = 3$ and $\mu = 2$ DFs can be more clearly observed in Fig. 4(c), which depicts the subtraction of the $\mu = 3$ DF from the DF of each μ, for $\lambda = 2$. Moreover, the DF difference between μ values becomes smaller with increasing n, similarly to the $\lambda = 0$ and $\lambda = 1$ SWCs [see Fig. 4(a) and (b)], although not as significantly.

C. CONSIDERATIONS FOR MORE THAN TWO OCLs

Due to space constraints, it is not possible to include in this paper the analysis for more than two OCLs. Nevertheless, several important remarks should be pointed out, for the design of a fault-tolerant drive, regarding greater numbers of OCLs. Obviously, the DF is progressively reduced as the number of OCLs rises. On the other hand, since it has already been shown that, broadly speaking, the main conclusions about the relation of the DF with λ and n are valid for either one or two OCLs, it can also be expected that, roughly, they also hold for other numbers of OCLs. Nonetheless, even if there are scenarios where they do not, the relevance of this fact would be relatively small, given that single or double OCLs are typically more probable, and hence the performance in these cases should be favored in the drive design.

IV. ANALYSIS OF SCL FOR TWO OCLs

Fig. 5 represents for each μ the normalized (by rated healthy conditions) SCL obtained with $\lambda = 1$ and $\lambda = 2$ at a torque value equal to the MAT of the star SWC for the same μ. Note that, accordingly, for $\lambda = 2$ no values are computed when the DF is lower than for star. In these conditions, it can be seen that $\lambda = 1$ yields the smallest losses, followed by $\lambda = 2$. Next, to evaluate the difference between SWCs, for each μ and n pair, in terms of SCL for a broad range of torque values, the ratio [8]

$$\eta_{\lambda,1} = \int_0^{\delta_\lambda i^{\mathrm{rc}}} \frac{J_\lambda}{J_1} d|i_{\alpha\beta_1}| \tag{4}$$

is employed, where i^{rc} denotes peak rated current, J_λ and J_1 represent the SCL for λ (any value) and $\lambda = 1$, respectively, and δ_λ is the DF for λ SWC. Equation (4) is individually calculated for each $\lambda \neq 1$, μ and n. Note that $\lambda = 1$ is taken as a reference in the denominator of (4) because, as in [8], $\lambda = 1$ offers higher DF and hence it is ensured that the integral can be computed up to $|i_{\alpha\beta_1}| = \delta_\lambda i^{\mathrm{rc}}$. From Fig. 6, the overall SCL is significantly lower for $\lambda = 1$ than for $\lambda = 0$ ($\eta_{\lambda,1} > 1$); it is also lower than for $\lambda = 2$, although this difference ($\eta_{\lambda,1}$ value) becomes small as n rises, particularly for $n > 10$. Therefore, the $\lambda = 1$ SWC is also preferable concerning SCL (as it was for DF), and for roughly $n > 10$ the $\lambda = 2$ SWC is similarly as good as $\lambda = 1$ in this regard. These outcomes are similar to those drawn in the preceding section in terms of DF, and also to those for single OCL [8]. Nevertheless, comparison of Fig. 6 and [8, Fig. 6] reveals that the improvement in SCL provided by $\lambda = 1$ (or $\lambda = 2$, at high n) with respect to star for two OCLs is in many cases even greater than for one OCL. For instance, for two OCLs the largest $\eta_{\lambda,1}$ with $\lambda = 0$ is 1.94 p.u. ($n = 6$ and $\mu = 1$), whereas for single OCL it is 1.26 p.u. ($n = 6$) [8].

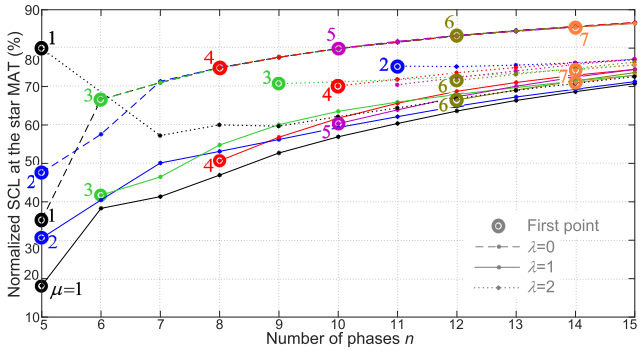

FIGURE 5. Normalized SCL of the $\lambda = 0$ (dashed), $\lambda = 1$ (solid) and $\lambda = 2$ (dotted) SWCs, obtained at torque equal to the MAT of the star SWC.

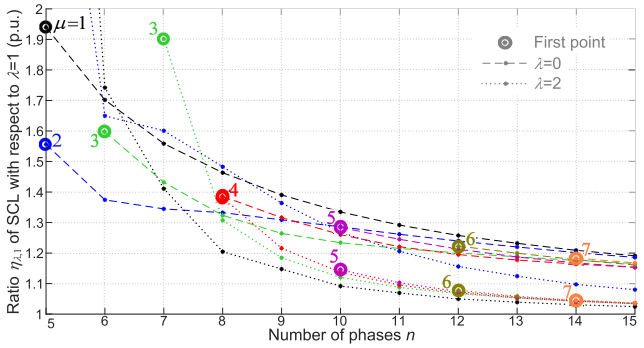

FIGURE 6. SCL ratio $\eta_{\lambda,1}$, for λ equal to 0 (dashed) or 2 (dotted) in (4).

To evaluate the SCL variation with μ per scenario, two ratios are defined, analogously to (4) but replacing λ by μ:

$$\eta_{\mu,1} = \int_0^{\delta_{\mu,1} i^{\mathrm{rc}}} \frac{J_\mu}{J_1} d|i_{\alpha\beta_1}|; \quad \eta_{\mu,2} = \int_0^{\delta_{\mu,2} i^{\mathrm{rc}}} \frac{J_\mu}{J_2} d|i_{\alpha\beta_1}| \qquad (5)$$

where J_μ, J_1 ad J_2 represent the SCL for μ (any value), $\mu = 1$ and $\mu = 2$ respectively, $\delta_{\mu,1}$ is the minimum between the μ and $\mu = 1$ DFs, and $\delta_{\mu,2}$ is the minimum between the μ and $\mu = 2$ DFs. The ratios in (5) are computed each time for given μ, λ and n. Since, as shown in Section III-A, $\mu = 2$ yields the largest DF (or nearly) with $\lambda = 0$ and $\lambda = 1$ for each n, $\eta_{\mu,2}$ is the figure adopted for evaluating the SCL with these two SWCs in Fig. 7(a) and (b). With $\lambda = 2$, $\mu = 3$ was shown to be preferable in terms of DF, but $\mu = 3$ is not valid for low n values; thus, $\eta_{\mu,1}$ is adopted in Fig. 7(c) to take $\mu = 1$ as a reference, which provides similar DF to $\mu = 3$ (see Fig. 2), especially for $n > 10$ (when $\lambda = 2$ is more attractive, as aforesaid).

From Fig. 7, the most convenient μ values regarding SCL are analogous to those established in Section III concerning DF. For $\lambda = 0$ and $\lambda = 1$, $\mu = 1$ and $\mu = 2$ are in general the worst and best possibilities in terms of SCL, respectively, although $\mu = 3$ is slightly (negligible) better in case of star SWC with $n \geq 8$. For $\lambda = 2$, the highest and lowest SCL is that of $\mu = 2$ and $\mu = 3$, respectively. Nonetheless, the SCL variation with μ becomes negligible as n approaches 15 for

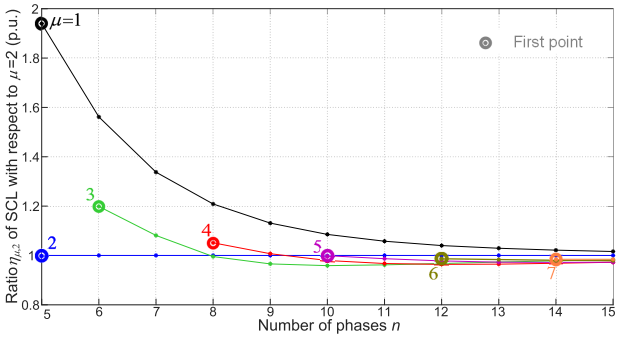

(a) Between each μ and $\mu = 2$ ($\eta_{\mu,2}$) for $\lambda = 0$ SWC.

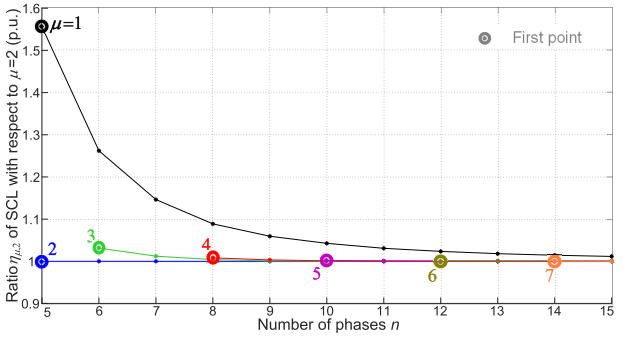

(b) Between each μ and $\mu = 2$ ($\eta_{\mu,2}$) for $\lambda = 1$ SWC.

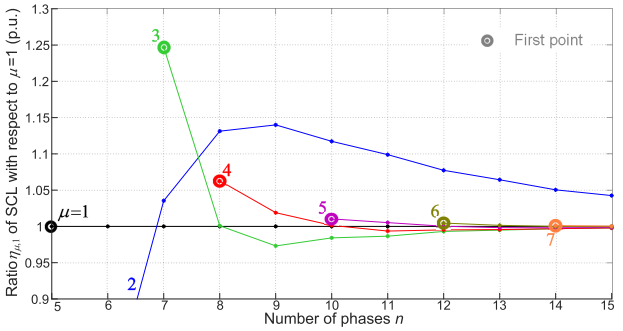

(c) Between each μ and $\mu = 1$ ($\eta_{\mu,1}$) for $\lambda = 2$ SWC.

FIGURE 7. SCL comparison between different μ, for each SWC.

any λ, although for $\lambda = 2$ with $\mu = 2$ the reduction with n is not as considerable.

V. ANALYSIS OF CONVERTER RATING FOR TWO OCLs

As mentioned in Section II-B, it is recommendable to set voltage and current ratings for the converter higher than those required for healthy operation, so that the potential postfault MAT allowed by the machine can actually be achieved [8], [47]. In other words, the postfault torque derating of the drive is only caused by the nature of the machine itself (its phase-current rating cannot be exceeded), not the converter voltage/current limitations, since the converter is adequately overrated for this purpose, as discussed next.

As shown in [8], the same dc-link voltage is suitable for any SWC and either healthy or one-OCL operation, if the stator-impedance voltage drop is neglected in comparison with the back-electromotive force at high speeds.

This follows from the fact that the current reference in the flux/torque-producing plane α_1-β_1 is equal for healthy or faulted conditions, and hence the back-electromotive force is nearly identical as well. Moreover, the usual non-current-producing 0^+ voltage injection for maximum dc-link utilization [7], [57], [58] also helps to make this assumption valid, since it counteracts the postfault imbalance of the voltage references [8]. Based on the same reasoning, it is straightforward to conclude that for two OCLs the same (roughly) dc-link voltage as for one OCL is sufficient as well. Thus, the curves displayed in [8, Fig. 8] are also valid for the dc-link voltage required under two (or more) OCLs. To facilitate the analysis of the overall performance for two OCLs, this figure is reproduced here in Fig. 8, but omitting λ values other than those of interest (0, 1, 2). The $V_{\rm dc}$ values are normalized by twice the amplitude of the per-phase back-electromotive force E_ϕ, i.e., by $2E_\phi$.

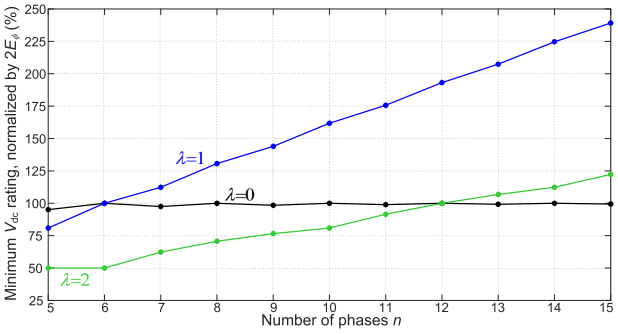

FIGURE 8. Required dc-link voltage $V_{\rm dc}$. Neglecting the stator-impedance voltage drop, these plots are valid for healthy drive or (roughly) OCLs [8].

Fig. 9 shows the required converter (line) current rating, normalized by the machine rated current $i^{\rm rc}$, for healthy (solid), single-OCL (dashed) and double-OCL (dotted) conditions. The curves for healthy drive and one OCL were assessed in [8], and are included here just for the sake of comparison with two OCLs. Since for two OCLs the line current depends on μ, the worst μ case is considered for each combination of n and λ. From Fig. 9, for $\lambda \neq 0$ with practically any n, double OCL implies greater current rating than single OCL. It can also be observed that in general for $\lambda \neq 0$ the necessary line current tends to decrease with increasing n; this is because the amplitude of the line current is given by $i^{\rm rc}\sqrt{2}\sqrt{1-\cos(\lambda 2\pi/n)}$ in healthy and rated conditions, and the behavior under one or two OCLs becomes closer to healthy as n rises.

Most importantly, Figs. 8 and 9 are useful for choosing n and λ, depending on the allowable voltage and current converter rating for a given fault-tolerant application. For the sake of illustration, let us consider that, e.g., the converter voltage and current rating should not be over 150% (of $2E_\phi$) and 200% (of the machine rated phase-current peak $i^{\rm rc}$), respectively, and that for each n the DF should be as high as possible while complying with these constraints. Note, from Section IV, that maximizing the DF normally also means

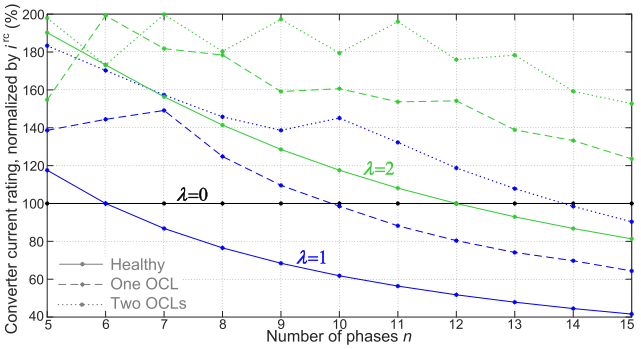

FIGURE 9. Required converter current rating for healthy (solid), single-OCL (dashed) and double-OCL (dotted) conditions.

minimizing (or nearly) the SCL. Permitting up to 200% current rating also makes it possible to tolerate faults with more than two OCLs; indeed, a line current, which for $\lambda \neq 0$ equals the subtraction of two stator phase currents (each of them limited to $2i^{\rm rc}$), cannot exceed $2i^{\rm rc}$, regardless of the number of OCLs. With these specifications in mind, it follows from Figs. 2, 6, 8 and 9 that the advisable options for this example are $\lambda = 1$ for $n < 10$, $\lambda = 0$ for $n = 10$, and $\lambda = 2$ for $n > 10$. This matches the choices recommended in [8] for single OCL. If instead, e.g., no more than 160% converter current rating is desired (together with the 150% voltage limitation) for tolerating two OCLs with maximum DF, then the preferred alternatives are $\lambda = 1$ for $n = 7, 8, 9$, $\lambda = 2$ for $n = 14, 15$, and $\lambda = 0$ for other n.

VI. PROPOSED RECONFIGURATION METHOD TO IMPROVE THE PERFORMANCE WITH TWO OCLs

In this section, based on the previous analysis, it is proposed to alter the connections between converter and machine, whenever two OCL faults have occurred with certain low-performance μ values, so that instead μ takes the values that yield the highest performance. In this manner, the DF and SCL are improved for given machine and faulted converter. This reconfiguration can be applied when two OCLs are present, regardless of whether the two OCL faults have occurred simultaneously or separated in time. Namely, in view of the outcomes of Sections III and IV, the modifications of μ displayed in Table 1 are proposed. The effective μ is modified from those in the third column to those in the fourth column (target μ), by means of an electric scheme of the type indicated in the last column, inserted between the machine and converter. When the not-equal sign is used in the table for the target μ, it means that any other μ values are advisable. Four types of schemes are proposed: A, B, C and D. Only reconfigurations such that the DF is increased in more than 5% (cf. Fig. 4) are included in Table 1; e.g., this is why $n = 15$ is ignored. For original μ values not reflected in the table, no reconfiguration is proposed. Although for $n \leq 10$ with $\lambda = 2$ there are some other cases where DF improvement above 5% can be attained, they are not shown in Table 1 either, because, as discussed in Sections III and IV, the DF and SCL

TABLE 1. Proposed Modifications of μ.

λ	n	Original μ	Target μ	Proposed scheme
0	5-7	1	2	Type A
0	8-10	1	3	Type D
1	5, 8-9	1	2	Type A
1	6	1, 3	2	Type B
1	7	1, 3	2	Type A
2	11	2, 5	$\neq 2, 5$	Type C
2	12-14	2	$\neq 2$	Type A

in such conditions are worse than with $\lambda = 0$, 1 and the same n value.

The μ change is performed by using additional bidirectional switches or solid-state relays (henceforth, "relays"). For given n, a scheme of type A is obtained by the following steps.

1) Use $\lfloor n/4 \rfloor$ blocks like the one shown in Fig. 10(a) for the first $4\lfloor n/4 \rfloor$ lines.
2) The remainder of $n/4$ is calculated: $\text{mod}(n/4) = n - 4\lfloor n/4 \rfloor$; depending on this value, the suitable scheme from Fig. 10(b)-(d) is applied to the last $\text{mod}(n/4)$ legs. In particular, that in Fig. 10(b), (c) or (d) is adopted when $\text{mod}(n/4)$ is equal to 1, 2 or 3, respectively.

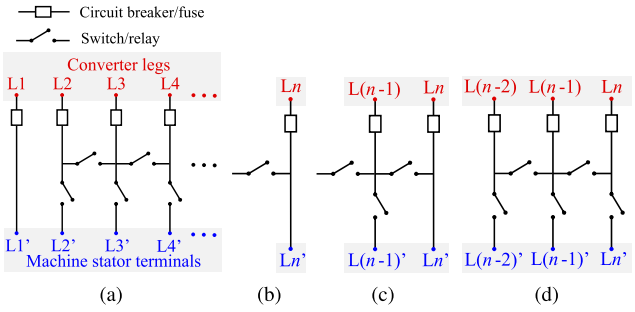

FIGURE 10. Proposed scheme of type A, for (a) the first $4\lfloor n/4 \rfloor$ lines (scheme repeated $\lfloor n/4 \rfloor$ times), and for the last $\text{mod}(n/4)$ lines when $\text{mod}(n/4)$ is equal to (b) 1, (c) 2 or (d) 3.

The number of extra relays necessary for type-A schemes is $5\lfloor n/4 \rfloor$ in case $\text{mod}(n/4) = 0$, and $5\lfloor n/4 \rfloor + 2\text{mod}(n/4) - 1$ otherwise. Note that no relays are needed, e.g., in the first line. The high-speed circuit breakers or fuses indicated for each leg at the top of the diagram are not a new proposal; they are often included in actual drives [9], [32], [47], [48].

The resulting schemes of type A for the particular cases of $n = 5, 6, 7, 9, 12$ are depicted in Fig. 11. Table 2 shows the states of the relays for the $n = 5$ structure in various scenarios. In agreement with Table 1, for $n = 5$ the drive behavior should only be altered by the scheme when $\mu = 1$. When this does not occur (see the second row of Table 2), the relays with odd number (S1, S3, S5), which are placed in series in a single line, are closed (indicated by 1); conversely, the relays with even number (S2, S4, S6), which can connect different lines, are open (indicated by 0). When $\mu = 1$, the procedure to change to $\mu = 2$ is based on opening

TABLE 2. Examples of Proposed Switch/Relay States for Fig. 11(a).

OCLs	S1	S2	S3	S4	S5	S6
$\mu \neq 1$, or not 2 OCLs	1	0	1	0	1	0
L1, L2	1	1	0	0	1	0
L2, L3	1	0	1	1	0	0
L3, L4	0	1	1	0	1	0
L4, L5	1	0	0	1	1	0
L5, L1	1	0	1	0	0	1

the odd-number relay of a healthy line that is adjacent to a faulted line, and closing the even-number relay that connects both lines. For instance, from Table 2, when L1 and L2 of Fig. 11(a) are OCLs, then S3 is turned off and S2 is turned on; hence, the system then behaves as if instead L1 and L3 ($\mu = 2$) were OCLs, yielding for $\lambda = 0$ an improvement of 17.1% in DF [see Fig. 4(a)], as well as a considerable reduction in SCL [see Fig. 7(a)]. This example of scheme reconfiguration is illustrated in Fig. 12. Analogous approaches can also be easily applied to conveniently modify μ for the other n, λ and fault scenarios where type-A schemes are suitable according to Table 1. In the cases of $n = 12, 13, 14$ with $\lambda = 2$, where $\mu \neq 2$ is recommended (see the last row), μ can also be changed in a similar manner from $\mu = 2$ to $\mu = 1$ or to $\mu = 3$ ($\mu \neq 2$).

Concerning the proposed scheme of type B, it is only needed for $n = 6$ (with $\lambda = 1$), as indicated in Table 1. This scheme is illustrated in Fig. 13. The only difference compared with Fig. 11(b) is that there is an extra relay (S9) next to L6'. S9 is opened if L2 and L5 are OCLs, so that the current in L6' is ceased and that in L5' is restored (closing S8). In this manner, in effect $\mu = 3$ is replaced by $\mu = 2$. Note that, e.g., when $\mu = 1$ is changed to $\mu = 2$ by using this scheme, the DF can be increased in as much as 28.9% [see Fig. 4(b)].

The type-C scheme, shown in Fig. 14, can be employed for $n = 11$ with $\lambda = 2$ to modify μ so that $\mu \neq 2, 5$ (see Table 1). In particular, μ is changed from 2 to 1 or 3, or from 5 to 4.

The schemes of type D for $n = 8, 9, 10$ are shown in Fig. 15. To allow replacing $\mu = 3$ by $\mu = 1$ (see Table 1), in this case relays are placed not between lines corresponding to adjacent legs (e.g., L3 and L4), but between lines of the same parity (e.g., L2 and L4).

In spite of the benefits of the proposed schemes, they also have some drawbacks that should be taken into account. Since extra devices are needed (numbers given in Table 3), the overall cost, size and complexity of the system is expected to moderately increase. Nevertheless, this is of relatively small relevance when high postfault performance is a priority. In fact, including extra bidirectional switches in order to enable (other) beneficial fault-tolerant reconfigurations is commonly done and considered advantageous in ac drives [1], [5], [16], [29], [37], [46]–[48], [59]–[62]. On the other hand, these additional elements can also fail. During normal (e.g., healthy) operation, if one of the relays next (in series) to the stator terminals becomes short circuited due to a failure, the performance is unaltered, whereas if it is open,

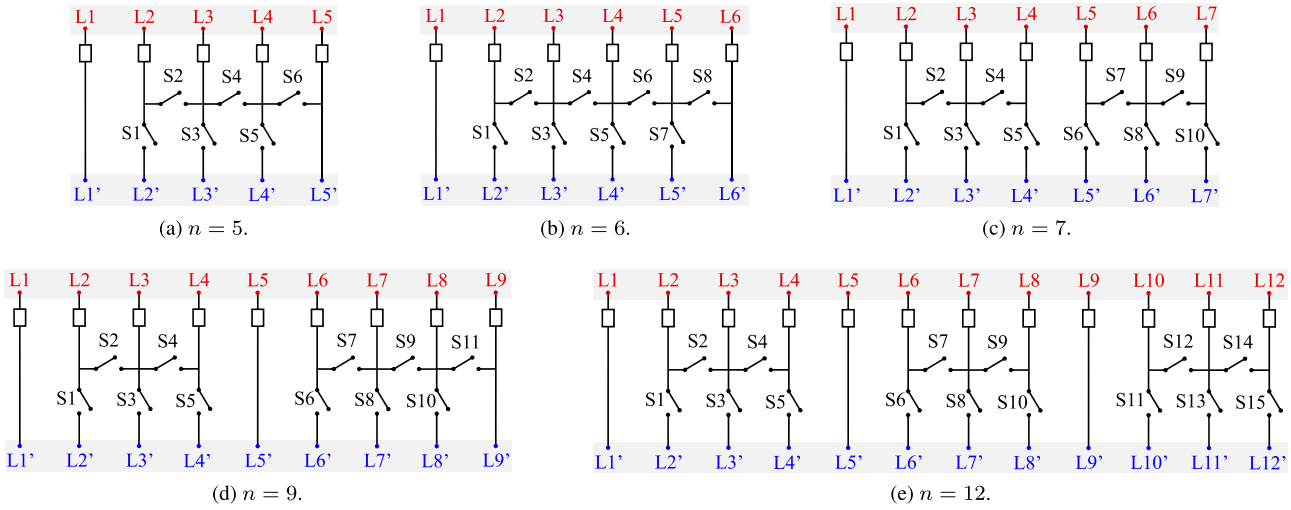

FIGURE 11. Examples of the proposed scheme of type A.

TABLE 3. Number of Extra Relays/Switches With Proposed Schemes.

λ	n	Scheme	Fig.	Extra relays
0,1	5	Type A	11(a)	6
0	6	Type A	11(b)	8
0,1	7	Type A	11(c)	10
0	8	Type D	15(a)	10
0	9	Type D	15(b)	12
0	10	Type D	15(c)	14
1	6	Type B	13	9
1	8	Type A	10	10
1	9	Type A	11(d)	11
2	11	Type C	14	16
2	12	Type A	11(e)	15
2	13	Type A	10	16
2	14	Type A	10	18

the effect is similar to an OCL; nevertheless, open-circuit faults are much less frequent than short-circuit ones in transistors (e.g., those in solid-state relays) [63]. Regarding the relays between lines, an open-circuit failure normally does not affect the system behavior, and suitable protective fuses can be inserted in series with these relays to interrupt the connection in case they suffer a short-circuit fault. Consequently, even if faults arise in the proposed schemes, this is unlikely to result in worse performance than in absence of such schemes. In any case, even if adding extra switches is not deemed worthy for a certain application, the analysis and proposals presented here are still useful; mainly in the sense that they allow a remarkable improvement in DF and SCL even if the reconfiguration is done off-line manually.

VII. EXPERIMENTAL RESULTS

In the following, experimental results obtained with six- and twelve-phase drives with symmetrical winding arrangement are presented. The interest of these two particular kinds of multiphase drives is evinced, e.g., by the attention they receive in relatively recent journal papers such as [8], [9], [33], [40], [64]–[71] and [8], [71], [72], respectively. This is due to, e.g., advantages over asymmetrical windings such as, as aforementioned, superior postfault performance [9], [25].

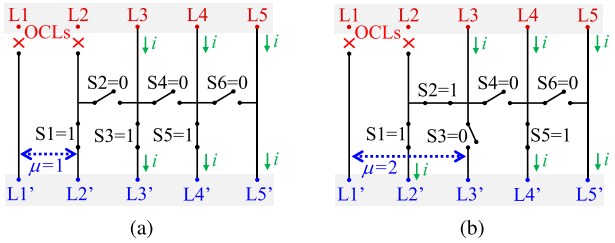

FIGURE 12. Example of proposed reconfiguration for $n = 5$ with OCLs in L1 and L2, from (a) $\mu = 1$ to (b) $\mu = 2$, using the scheme from Fig. 11(a) in accordance with Table 2.

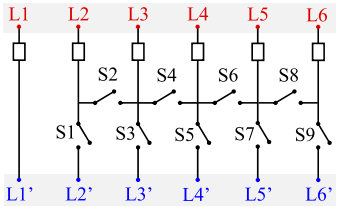

FIGURE 13. Proposed scheme of type B, for $n = 6$ with $\lambda = 1$.

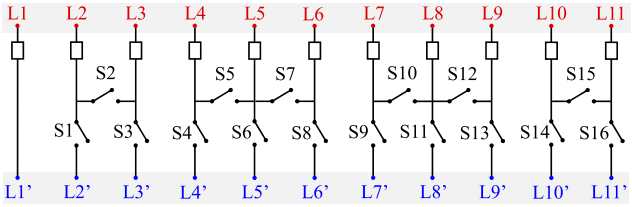

FIGURE 14. Proposed scheme of type C, for $n = 11$ with $\lambda = 2$.

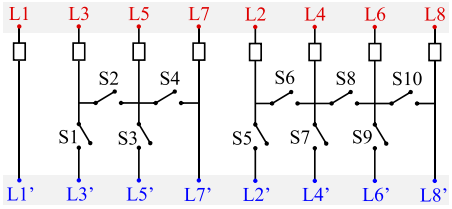

(a) $n = 8$.

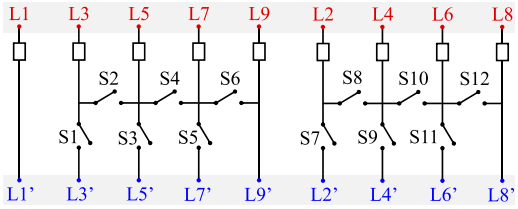

(b) $n = 9$.

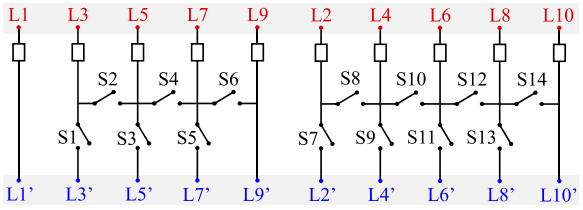

(c) $n = 10$.

FIGURE 15. Proposed scheme of type D.

A. EXPERIMENTAL RESULTS WITH SIX-PHASE INDUCTION MOTOR

1) EXPERIMENTAL SETUP

The experimental setup consists of a symmetrical six-phase induction machine with an eddy-current brake, used to regulate the load torque. A torque transducer is also included. A photograph of the control platform and converter can be seen in [37, Fig. 13(b)], and of the test bench in [8, Fig. 10(a)]. The speed is maintained at 1500 r/min in closed loop by a dSPACE-DS1006 platform, including an inner field-oriented current controller. Resonant current controllers (equivalent to synchronous proportional-integral ones) are implemented at the fundamental [6], [19], [20] and low-order harmonic [18], [58], [73] frequencies. The switching frequency of the two-level inverter is 10 kHz. The switching harmonics are removed from the measured currents by applying oversampling and averaging [8], [58], [74], [75]. The dc-link voltage is kept at 350 V. The six-phase motor has stator and rotor resistance of 6.9 Ω and 6.3 Ω, respectively, magnetizing inductance of 652 mH, stator and rotor leakage inductance of 2.8 mH and 16.6 mH, respectively, and one pole pair. Through this section the current is normalized by its rated value, which is assumed to have an amplitude of $i^{\mathrm{rc}} = 2.7$ A.[3] Machine power and torque ratings of 1.3 kW and 4.78 Nm are considered, respectively. During the tests, the magnitude of the d-axis current is kept ($i_{\mathrm{d}} = 1$ A) and just that of the q-axis current i_{q} varies [6], [8], [10], [11], depending on the load. The configuration with each λ and μ is tested at the corresponding MAT and also at the MATs of all the other λ-μ cases, when feasible, in accordance with the DFs from Fig. 2. The respective i_{q} and torque values are reflected in Table 4 for this setup.

[3]This value is slightly less conservative than that (2.24 A) considered in [8], [54] for the same machine, because this increase is needed in order to run the motor with $\lambda = 2$ and $\mu = 1$ (DF of 43.3%), the actual rated current is not known precisely, and 2.7 A is not applied for a long time.

TABLE 4. Torque and i_{q} (while $i_{\mathrm{d}} = 1$ A) for Each $|i_{\alpha\beta_1}|$ Tested for $n = 6$.

$\lvert i_{\alpha\beta_1}\rvert$ (%)	43.3	50.0	57.7	66.6	86.6	100
λ-μ with such DF	2-1	0-1; 2-2	0-2; 0-3; 1-1	1-3	1-2	–
i_{q} (A)	0.61	0.91	1.19	1.49	2.11	2.51
Torque (Nm)	1.16	1.73	2.28	2.85	4.03	4.78
Torque (%)	24.1	36.2	47.6	59.6	84.3	100

In the first place, the drive is tested in healthy conditions at $|i_{\alpha\beta_1}| = 100\%$ (torque of 4.78 Nm) with each SWC. The values of SCL, line-current rms and line-to-line (among legs corresponding to the same loop or star) voltage-reference peak are displayed in Table 5. The line-to-line voltage peak represents the required dc-link voltage [8]. For the $\lambda = 1$ and $\lambda = 2$ SWCs, the SCL includes the losses due to currents circulating within the loops. Although it can be observed in this table that in healthy situation $\lambda = 2$ requires much greater line current and lower dc-link voltage (in agreement with Figs. 8 and 9), and that the circulating current is negligible, these facts were already known from [8]. The quantities shown in Table 5 will be useful next, for comparison with those obtained in each fault scenario.

TABLE 5. Experimental Performance Under Healthy Operation With $|i_{\alpha\beta_1}| = 100\%$ for $n = 6$.

Parameter	$\lambda = 0$	$\lambda = 1$	$\lambda = 2$
SCL (W)	150.6	150.8	149.6
Line-current rms (% of $i^{\mathrm{rc}}/\sqrt{2}$)	99.9	100	172
Line-to-line (within a loop or star) voltage-reference peak (V)	310	307	161

It should also be pointed out that, as commonly done in other papers about fault tolerance in multiphase drives [5], [6], [8], [19], [20], [24]–[26], [32], [37], [54], in the following the experimental phase-current waveforms are accompanied by the corresponding current trajectories per subspace. On the one hand, the current waveforms per phase make it possible to check the satisfaction of the current constraints, including the fault restrictions and the $i \leq i^{\mathrm{rc}}$ condition. On the other hand, the current trajectories per subspace show whether the α_1-β_1 current describes a circumference (no torque ripple), whose radius is $|i_{\alpha\beta_1}|$ (related to DF and MAT), and also how the current constraints make it necessary to impose certain current in other subspaces.

2) EVALUATION OF DF

Fig. 16 shows the steady-state stator phase current with $\lambda = 0$ SWC, for each of the scenarios of two faulty legs ($\mu = 1, 2, 3$), at the respective MATs (cf. Fig. 2), i.e., with $|i_{\alpha\beta_1}|$ of 50.0%, 57.7% and 57.7% (see the torque values in Table 4). The current is expressed as a percentage of i^{rc}. It can be seen that the healthy phases have current peaks roughly equal to rated (i.e., 100%), confirming that these $|i_{\alpha\beta_1}|$ values are the corresponding MATs, in accordance with [9] (which only considers $\lambda = 0$) and with the theory in this paper (cf. Fig. 2). Any attempt to further increase $|i_{\alpha\beta_1}|$ results in overcurrent in some phases. In the $\mu = 2$ case [see Fig. 16(b)], at the MAT not all the phase currents have peaks of 100%. This is because the combination of the 0^+ zero-sequence current restriction (the sum of all phase currents is zero [8]) with $\mu = 2$ does not allow to provide 100% current in all healthy phases. This is similar to the reason why $|i_{\alpha\beta_1}|$ cannot be made greater than 55.7% in six-phase machines with asymmetrical winding arrangement and phases a and c (also $2\pi/3$ apart) open [9], [26], despite the fact that only one of the six phases has then rated current [26].

The results for the $\lambda = 1$ and $\lambda = 2$ SWCs are shown in Figs. 17 and 18, respectively, also at the MAT for each possible μ. The peaks of the phase currents are roughly 100% of i^{rc} in every capture; the only exceptions are the phases connected to a faulty leg, due to the associated current constraints. Thus, the theoretical MAT (or DF) values from Fig. 2 are verified.

Most importantly, from Figs. 16-18 and Table 4, $\lambda = 1$ permits to achieve greater MAT than other SWCs for all the possible two-OCL scenarios in symmetrical six-phase machines, corroborating the theoretical findings from Section III. Another conclusion from the theory (from Section III-A) that is now confirmed is the fact that in general $\mu = 1$ and $\mu = 2$ are the least and most convenient cases for $\lambda = 0, 1$. Indeed, Figs. 16(a) and 17(a) reflect the lowest MAT for $\lambda = 0$ and $\lambda = 1$ (50% and 57.7%, i.e., 0.91 Nm and 1.19 Nm), respectively, whereas Figs. 16(b) and 17(b) correspond to the largest MAT (57.7% and 86.6%, i.e., 1.19 Nm and 2.11 Nm) for each SWC. Although for $n = 6$ with star, $\mu = 2$ does not yield higher MAT than $\mu = 3$, that of the latter is not greater either. Concerning $\lambda = 2$, in this case $\mu = 2$ is also preferable over $\mu = 1$, but for $n = 6$ this SWC is not recommendable, due to its much smaller MATs compared with $\lambda = 0, 1$. These assessments about the superiority of $\lambda = 1$ and $\mu = 2$ also reinforce the convenience of the proposal (for $n = 6$ with $\lambda = 1$) from Section VI to change from $\mu = 1, 3$ to $\mu = 2$.

3) EVALUATION OF SCL

Table 6 displays the SCL obtained experimentally, including that due to (if any) circulating currents. Each configuration (μ and λ pair) is also tested at the MATs of the other ones, when possible. From this table, the SCL for $\lambda = 1$ is lower than for the other SWCs in all $|i_{\alpha\beta_1}|$ cases where they are feasible. It can also be seen that, for any

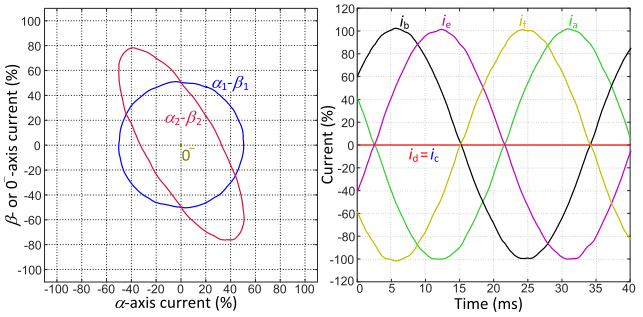

(a) Lines L3 and L4 open ($\mu = 1$), with $|i_{\alpha\beta_1}| = 50.0\%$.

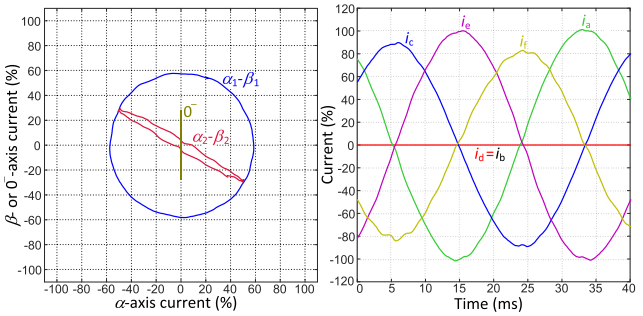

(b) Lines L2 and L4 open ($\mu = 2$), with $|i_{\alpha\beta_1}| = 57.7\%$.

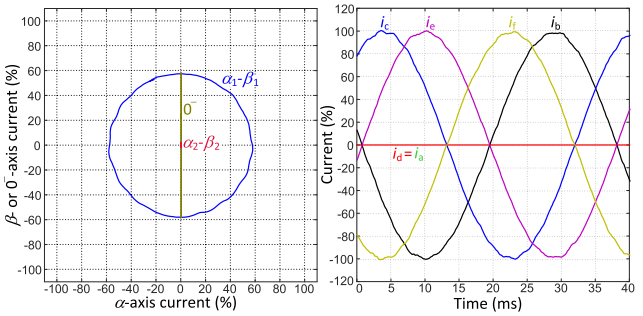

(c) Lines L1 and L4 open ($\mu = 3$), with $|i_{\alpha\beta_1}| = 57.7\%$.

FIGURE 16. Experimental stator phase current for $n = 6$ with $\lambda = 0$ (star) SWC, at the MAT of each fault scenario.

TABLE 6. Experimental SCL (in W) for $n = 6$.

$\lvert i_{\alpha\beta_1}\rvert$	$\lambda = 0$ SWC			$\lambda = 1$ SWC			$\lambda = 2$ SWC		
	$\mu = 1$	$\mu = 2$	$\mu = 3$	$\mu = 1$	$\mu = 2$	$\mu = 3$	$\mu = 1$	$\mu = 2$	$\mu = 3$
43.3%	75.3	46.3	57.4	43.3	34.0	35.8	75.7	56.7	–
50.0%	102.1	63.3	76.3	57.7	45.8	46.9	–	74.9	–
57.7%	–	86.9	99.6	85.3	60.7	62.3	–	–	–
66.6%	–	–	–	–	81.0	83.8	–	–	–
86.6%	–	–	–	–	148.7	–	–	–	–

$|i_{\alpha\beta_1}|$ and SWC, the SCL for $\mu = 2$ is lower than for other μ. That is, the cases that are preferable in terms of MAT (just assessed in Section VII-A2) are also advantageous regarding SCL, as expected from theory.

4) EVALUATION OF REQUIRED CONVERTER RATING

The maximum line current rms among the converter lines, in each experimental scenario, is shown (normalized) in Table 7. Obviously, for $\lambda = 0$ the line currents are equal

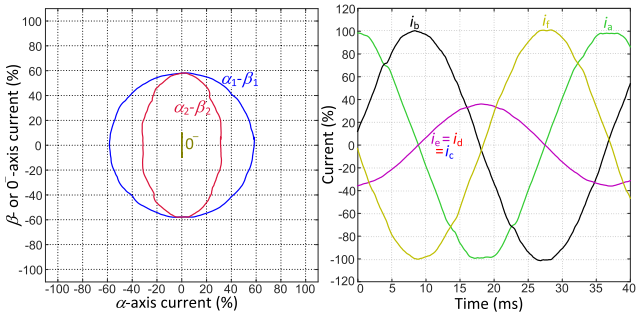

(a) Lines L3 and L4 open ($\mu = 1$), with $|i_{\alpha\beta_1}| = 57.7\%$.

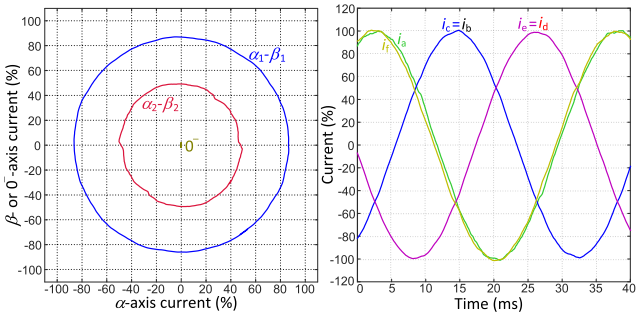

(b) Lines L2 and L4 open ($\mu = 2$), with $|i_{\alpha\beta_1}| = 86.6\%$.

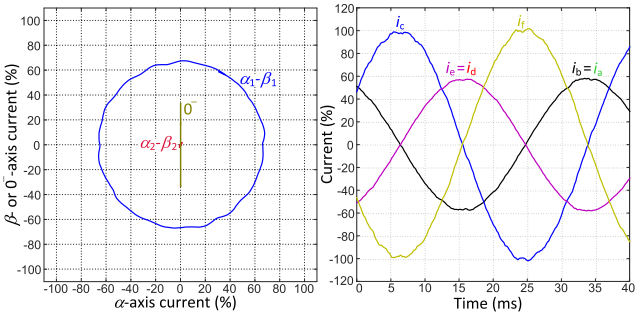

(c) Lines L1 and L4 open ($\mu = 3$), with $|i_{\alpha\beta_1}| = 66.6\%$.

FIGURE 17. Experimental stator phase current for $n = 6$ with $\lambda = 1$ SWC, at the MAT of each fault scenario.

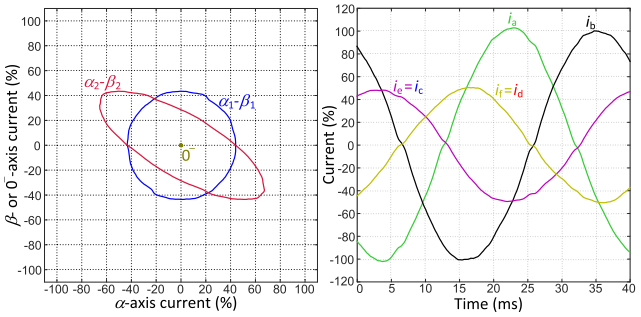

(a) Lines L2 and L3 open ($\mu = 1$), with $|i_{\alpha\beta_1}| = 43.3\%$.

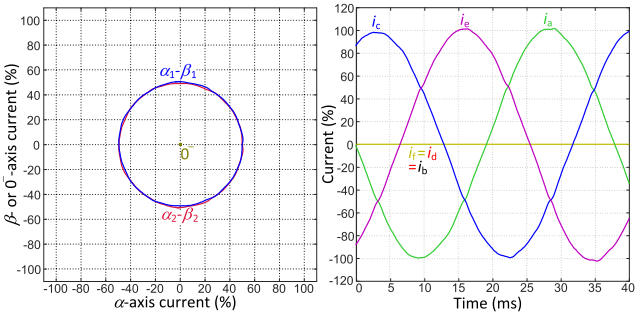

(b) Lines L2 and L4 open ($\mu = 2$), with $|i_{\alpha\beta_1}| = 50.0\%$.

FIGURE 18. Experimental stator phase current for $n = 6$ with $\lambda = 2$ SWC, at the MAT of each fault scenario.

TABLE 7. Experimental Line-Current RMS (% of $i^{\mathrm{rc}}/\sqrt{2}$) for $n = 6$.

$\lvert i_{\alpha\beta_1}\rvert$	$\lambda = 0$ SWC			$\lambda = 1$ SWC			$\lambda = 2$ SWC		
	$\mu = 1$	$\mu = 2$	$\mu = 3$	$\mu = 1$	$\mu = 2$	$\mu = 3$	$\mu = 1$	$\mu = 2$	$\mu = 3$
43.3%	92.7	75.4	75.7	92.7	76.0	75.8	150.7	151.0	–
50.0%	100.9	88.6	87.2	106.5	87.9	86.5	–	172.9	–
57.7%	–	99.7	100.1	140.0	101.6	100.1	–	–	–
66.6%	–	–	–	–	116.8	115.7	–	–	–
86.6%	–	–	–	–	172.1	–	–	–	–

TABLE 8. Experimental Line-to-Line (Within a Loop or Star) Voltage-Reference Peak (in V) for $n = 6$.

$\lvert i_{\alpha\beta_1}\rvert$	$\lambda = 0$ SWC			$\lambda = 1$ SWC			$\lambda = 2$ SWC		
	$\mu = 1$	$\mu = 2$	$\mu = 3$	$\mu = 1$	$\mu = 2$	$\mu = 3$	$\mu = 1$	$\mu = 2$	$\mu = 3$
43.3%	272	289	297	271	284	291	164	158	–
50.0%	271	288	291	273	277	285	–	157	–
57.7%	–	293	295	260	277	285	–	–	–
66.6%	–	–	–	–	280	290	–	–	–
86.6%	–	–	–	–	291	–	–	–	–

to the phase currents. The highest rms values in the table are nearly 172% (for $\lambda = 1, 2$), which are very close to the respective ones displayed in Fig. 9, which were found theoretically. Although $\lambda = 1$ implies greater converter current rating than $\lambda = 0$, this shortcoming is expected to be acceptable when postfault performance in terms of MAT and SCL is a priority [8]. It is also worth noting that, although $\mu = 2$ requires greater line current (for $\lambda = 1, 2$) than $\mu = 1, 3$, the converter should nevertheless be overrated for the worst-case scenario, i.e., by roughly 72%, even if eventually a fault with $\mu = 2$ does not arise. Consequently, the converter current rating when using the scheme proposed in Section VI to modify the operation from $\mu = 1, 3$ to $\mu = 2$ does not have to be higher than when such scheme is not adopted.

The peak values of the line-to-line (within a loop/star) voltage references in each case are shown in Table 8. As expected, these values, and hence also the required dc-link voltage, are similar to those at healthy conditions (cf. Table 5). If the stator impedance were not as large (it is a low-power non-optimized prototype), they would be even closer. Most importantly, note that, for $n = 6$, $\lambda = 1$ does not need higher dc-link voltage rating than $\lambda = 0$, in spite of the much better postfault performance of the former.

5) TRANSITION FROM $\mu = 1$ TO $\mu = 2$ WITH $\lambda = 1$ SWC

Fig. 19 shows the current waveforms obtained during the transition from $\mu = 1$ to $\mu = 2$ when the method proposed

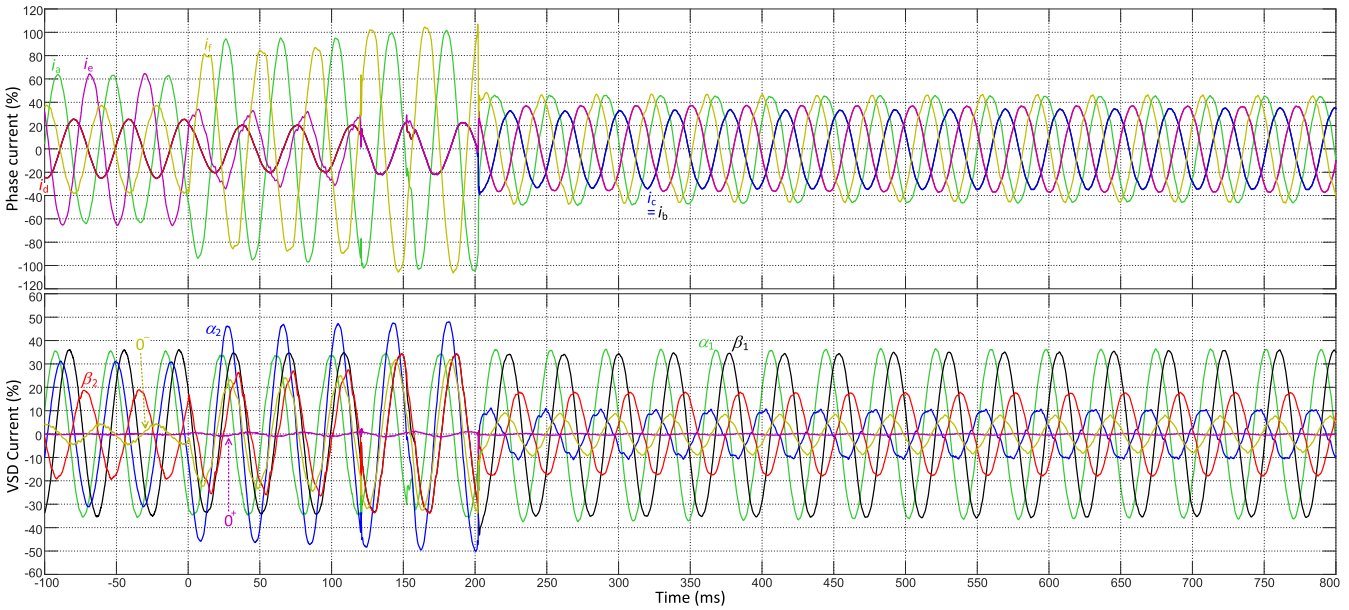

FIGURE 19. Experimental stator phase current during transition from $\mu = 1$ to $\mu = 2$, for $n = 6$ with $\lambda = 1$ SWC, OCLs in L2 and L3, and $|i_{\alpha\beta_1}| = 35.8\%$, by means of the method proposed in Section VI.

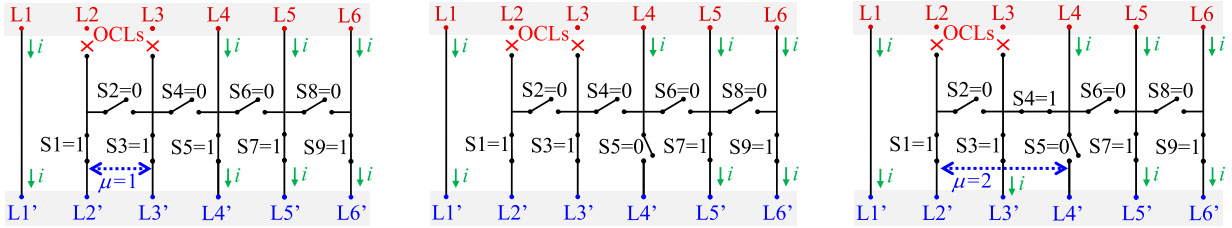

(a) $t < 120$ ms. (b) 120 ms $< t <$ 202 ms. (c) 202 ms $< t$.

FIGURE 20. Scheme of Fig. 13 during the experimental transition shown in Fig. 19 for $n = 6$ with OCLs in L2 and L3, from $\mu = 1$ to $\mu = 2$, in agreement with the contactor states displayed in Table 9.

in Section VI is applied, with $\lambda = 1$ SWC. The scheme illustrated in Fig. 13 is employed. The OCLs are those of lines L2 and L3. Contactors Schneider Electric LC1D18BL are used as bidirectional switches S1-S9. Their states S1-S9 during the transition are displayed in Table 9, as well as the commands for contactors S4 and S5 (denoted by S4' and S5', respectively). All the delays shown in Table 9 between a command (S4' or S5') modification and the actual change of the corresponding contactor state (S4 or S5) are due to the inherent delays of the contactors. It can also be noted in this table that S4' is not activated until S5 has been effectively opened, to prevent short circuits. The scheme from Fig. 13 in each stage of the transition, in accordance with the contactor states S1-S9 from Table 9, is illustrated in Fig. 20. In addition, Table 10 reflects the constraints imposed by the faults and by the contactor states on the stator phase currents for each of the steps shown in Fig. 20. These constraints are easily obtained by inspection of Figs. 1(b) and 20.

Initially, the odd- and even-number contactors are closed and open, respectively [see Table 9 and Fig. 20(a)], as in healthy situation. Accordingly, at the beginning the currents

TABLE 9. Contactor States S1-S9 and Commands S4'-S5' During Transition Shown in Fig. 19 Using the Scheme From Fig. 13.

	S1	S2	**S3**	**S4**	**S4'**	**S5**	**S5'**	S6	S7	S8	S9
$t < 0$ ms	1	0	**1**	**0**	**0**	**1**	**1**	0	1	0	1
0 ms $< t <$ 120 ms	1	0	**1**	**0**	**0**	**1**	**0**	0	1	0	1
120 ms $< t <$ 202 ms	1	0	**1**	**0**	**1**	**0**	**0**	0	1	0	1
202 ms $< t$	1	0	**1**	**1**	**1**	**0**	**0**	0	1	0	1

TABLE 10. Fault Phase-Current Constraints During Transition Shown in Fig. 19.

	Fault phase-current constraints
$t < 120$ ms	$i_b = i_c;\ i_c = i_d$
120 ms $< t <$ 202 ms	$i_b = i_c;\ i_c = i_d;\ i_d = i_e$
202 ms $< t$	$i_b = i_c;\ i_d = i_e$

of phases b, c and d are identical in Fig. 19, due to the faults. The load is such that $|i_{\alpha\beta_1}| = 35.8\%$. The transition starts at $t = 0$ s. At this instant, the contactor in series with L4'

TABLE 11. Torque, i_d and i_q for Each $|i_{\alpha\beta_1}|$ Tested for $n = 12$.

$\lvert i_{\alpha\beta_1}\rvert$ (%)	78.0	79.6	80.6	81.1	81.5	82.0	84.0	91.1	91.9	94.9	95.3	97.1	98.7	98.8	98.9	100
λ-μ with such DF	0-1	0-2	0-6	0-5	0-3	0-4	2-2	2-6	2-1;2-5	2-4	2-3	1-1	1-6	1-5	1-2,3,4	–
$-i_d$ (mA)	108	112	115	116	117	119	125	147	149	159	161	167	172	173	173	177
i_q (A)	4.41	4.50	4.56	4.59	4.61	4.64	4.75	5.15	5.20	5.37	5.39	5.49	5.58	5.59	5.59	5.65
Torque (Nm)	54.8	55.9	56.6	57.0	57.3	57.6	59.0	64.0	64.6	66.7	67.0	68.2	69.4	69.4	69.5	70.3
Torque (%)	78.0	79.6	80.6	81.1	81.5	82.0	84.0	91.1	91.9	94.9	95.3	97.1	98.7	98.8	98.9	100

(i.e., S5) is commanded to open, and the current references are modified so that the line currents of L2', L3' and L4' (not just L2' and L3', as before) are zero, according to the full-range minimum loss strategy [8]. S5 takes some time (until $t = 120$ ms) to open in practice, and in the interim the current control ensures (tracking the new references) that the L4' line current is already nearly zero [$i_e \approx i_d$; cf. Fig. 1(b)]. From $t = 120$ ms on, it is effectively open ($i_e = i_d$), with the only exception of a brief bounce of the contactor at around $t = 152$ ms. The contactor between L3' and L4' (i.e., S4 in Fig. 20) is commanded to close at $t = 120$ ms, and its closure occurs at $t = 202$ ms. Immediately, the current references are set for SCL minimization [8] while obeying the restriction that the L2' and L4' line currents are zero ($i_b = i_c$ and $i_d = i_e$), but no longer the L3' one. Note that this reference change may be applied later, if the instant of S4 closure is unknown.

Most importantly, from Fig. 19, the transition is done in a relatively short time and without excessive current peaks, and as intended the proposed modification from $\mu = 1$ to $\mu = 2$ permits to obtain considerably smaller phase currents than initially (for given $|i_{\alpha\beta_1}|$, i.e., flux and torque). If solid-state relays or triacs are employed instead of electromechanical contactors, the transition time may be even further reduced.

Although this setup is a low-power prototype, it should be remarked that opening a contactor during operation is not expected to be troublesome, even in high-power drives, provided the corresponding current is set to zero beforehand by means of the current control, as done here, and its disturbance-rejection capability is properly designed. Moreover, fault-tolerant multiphase drives are also of interest in practical applications of relatively low power where reliability is important (e.g., standalone generators [5]).

Concerning the transition from healthy to faulty operation, it has been addressed in previous publications [17], [19], it is out of the scope of this paper, and the resonant (or equivalent proportional-integral) current controllers used here are suitable for this purpose, provided a fault detection algorithm is also included [17], [19].

B. EXPERIMENTAL RESULTS WITH TWELVE-PHASE PERMANENT-MAGNET MACHINE

1) EXPERIMENTAL SETUP

Experimental tests are also carried out with a twelve-phase permanent-magnet synchronous machine working as a generator, as in [8] (setup shown in [8, Fig. 14]). This machine is coupled with a three-phase induction motor, driven by a commercial variable speed drive. The latter is configured so that, disregarding the slip, the shaft speed is 600 r/min. The active power absorbed by the generator is delivered to a resistive load, in parallel with the dc-link of the twelve-phase converter. The voltage of the dc link is 750 V. The twelve-phase machine is controlled by means of field-oriented control with maximum-torque-per-ampere strategy implemented in a dSPACE-MicroLabBox platform, using 5-kHz sampling and switching frequency. The generator has four pole pairs, stator resistance of 0.7 Ω, stator leakage inductance of 0.4 mH, d- and q-axis inductances of $L_d = 1.6$ mH and $L_d = 2.8$ mH, and voltage constant (phase voltage in rms) of 0.1533 V/r/min. Machine ratings of phase-current peak, torque and power of $i^{rc} = 5.66$ A, 70.3 Nm and 11 kW are considered, respectively.

Table 11 presents the torque and d/q-current values being tested. All these cases match the MAT of one of the λ-μ combinations for $n = 12$ (cf. Fig. 2).

The figures of merit at healthy conditions with $|i_{\alpha\beta_1}| = 100\%$ (torque of 70.3 Nm), shown in Table 12, are in agreement with the theory and with [8]. Mainly, circulating current is negligible, and the maximum line-to-line voltage and current peak are much higher for $\lambda = 1$ and for $\lambda = 2$, respectively (cf. Figs. 8 and 9). The moderate voltage discrepancies are especially due to harmonics/imbalance and the theoretical assumption of negligible stator-impedance voltage drop.

TABLE 12. Experimental Performance Under Healthy Operation With $|i_{\alpha\beta_1}| = 100\%$ for $n = 12$.

Parameter	$\lambda = 0$	$\lambda = 1$	$\lambda = 2$
SCL (W)	134.4	134.4	134.4
Line-current rms (% of $i^{rc}/\sqrt{2}$)	100.0	51.8	100.1
Line-to-line (within a loop or star) voltage-reference peak (V)	272	519	247

2) EVALUATION OF DF

It has been checked that, for $n = 12$, $\lambda = 0, 1, 2$ and every μ, the DFs match those assessed in Fig. 2. Since it is not possible to include captures for all cases, those corresponding to the largest MAT with $\lambda = 0$ ($\mu = 4$), $\lambda = 1$ ($\mu = 3$) and $\lambda = 2$ ($\mu = 3$) are shown in Figs. 21, 22 and 23, respectively. Note that all phase currents have peaks of roughly 100% (it is the MAT). As expected from Section III, the highest possible $|i_{\alpha\beta_1}|$ for $\lambda = 2$ (95.3%, i.e., 67.0 Nm) is close to

TABLE 13. Experimental SCL (in W) for $n = 12$.

$\lvert i_{\alpha\beta_1}\rvert$	$\lambda = 0$ SWC						$\lambda = 1$ SWC						$\lambda = 2$ SWC					
	$\mu = 1$	$\mu = 2$	$\mu = 3$	$\mu = 4$	$\mu = 5$	$\mu = 6$	$\mu = 1$	$\mu = 2$	$\mu = 3$	$\mu = 4$	$\mu = 5$	$\mu = 6$	$\mu = 1$	$\mu = 2$	$\mu = 3$	$\mu = 4$	$\mu = 5$	$\mu = 6$
78.0%	112.0	106.3	101.1	100.0	102.0	103.3	85.6	83.7	83.7	83.7	83.7	83.8	89.8	96.8	89.2	89.4	89.8	90.0
79.6%	–	111.9	105.8	104.3	107.0	108.4	89.2	87.1	87.1	87.2	87.2	87.2	93.5	100.9	92.9	93.1	93.5	93.7
80.6%	–	–	108.9	107.3	110.3	112.1	91.4	89.4	89.3	89.4	89.4	89.4	95.9	103.7	95.3	95.5	95.9	96.1
81.1%	–	–	110.5	108.8	112.1	–	92.5	90.5	90.5	90.5	90.5	90.5	97.1	105.1	96.5	96.7	97.1	97.3
81.5%	–	–	111.9	110.2	–	–	93.5	91.4	91.3	91.4	91.4	91.4	98.0	106.2	97.4	97.6	98.0	98.3
82.0%	–	–	–	112.0	–	–	94.6	92.5	92.5	92.5	92.5	92.5	99.3	107.7	98.6	98.8	99.3	99.5
84.0%	–	–	–	–	–	–	99.3	97.0	97.0	97.0	97.1	97.1	104.2	115.2	103.5	103.7	104.1	104.4
91.1%	–	–	–	–	–	–	116.8	114.1	114.1	114.1	114.2	114.2	125.1	–	121.7	122.1	125.1	132.3
91.9%	–	–	–	–	–	–	118.8	116.1	116.1	116.2	116.2	116.2	131.6	–	123.9	124.5	131.6	–
94.9%	–	–	–	–	–	–	126.9	123.9	123.8	123.9	123.9	123.9	–	–	133.1	134.4	–	–
95.3%	–	–	–	–	–	–	128.1	124.9	124.9	124.9	125.0	125.0	–	–	134.4	–	–	–
97.1%	–	–	–	–	–	–	134.3	129.7	129.6	129.7	129.8	129.8	–	–	–	–	–	–
98.7%	–	–	–	–	–	–	–	134.0	134.0	134.1	134.3	134.4	–	–	–	–	–	–
98.8%	–	–	–	–	–	–	–	134.3	134.3	134.4	134.5	–	–	–	–	–	–	–
98.9%	–	–	–	–	–	–	–	134.6	134.5	134.6	–	–	–	–	–	–	–	–

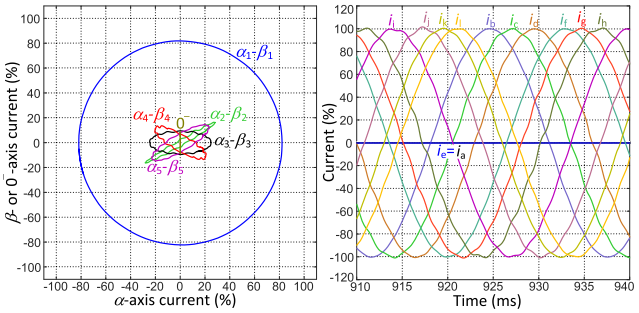

FIGURE 21. Experimental stator phase current for $n = 12$ with $\lambda = 0$ SWC, lines L1 and L5 open ($\mu = 4$), and $|i_{\alpha\beta_1}| = 82.0\%$ (the MAT).

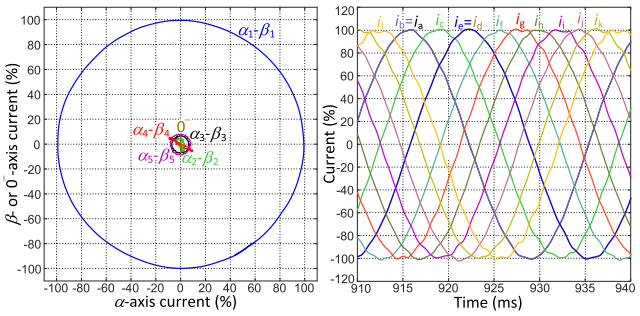

FIGURE 22. Experimental stator phase current for $n = 12$ with $\lambda = 1$ SWC, lines L1 and L4 open ($\mu = 3$), and $|i_{\alpha\beta_1}| = 98.9\%$ (the MAT).

that for $\lambda = 1$ (98.9%, i.e., 69.5 Nm), and much greater than for $\lambda = 0$ (82.0%, i.e., 57.6 Nm). The DFs of the other scenarios are also indirectly further corroborated by the following results.

3) EVALUATION OF SCL

The SCL for all the postfault tests is shown in Table 13. It can be observed that, for given $|i_{\alpha\beta_1}|$, the SCL is always smaller for the λ-μ pairs such that the DF (largest possible $|i_{\alpha\beta_1}|$ in the table) is higher, in agreement with the theoretical study from Section IV. For instance, taking $|i_{\alpha\beta_1}| = 78.0\%$ as an

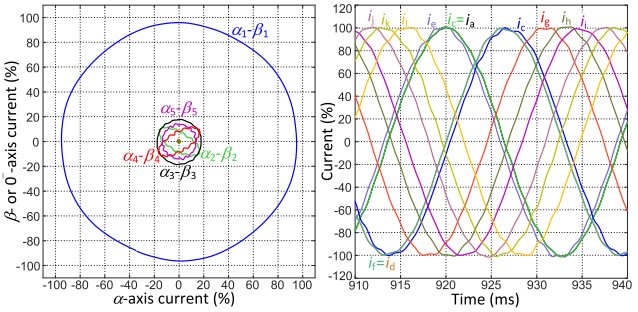

FIGURE 23. Experimental stator phase current for $n = 12$ with $\lambda = 2$ SWC, lines L1 and L4 open ($\mu = 3$), and $|i_{\alpha\beta_1}| = 95.3\%$ (the MAT).

example, the SCL is lower for $\lambda = 2$ with $\mu = 3$ (89.2 W) than for $\lambda = 2$ with $\mu = 2$ (96.8 W) or for $\lambda = 0$ with $\mu = 4$ (100.0 W), but relatively close to the SCL for $\lambda = 1$ with $\mu = 3$ (83.7 W). These observations confirm the following conclusions from the theory for $n = 12$ in terms of both SCL and DF: a) $\lambda = 2$ is preferable over $\lambda = 0$, but not too inferior with respect to $\lambda = 1$; b) for $\lambda = 2$, it is advisable to replace, as proposed, $\mu = 2$ by a $\mu \neq 2$ value such as $\mu = 3$.

4) EVALUATION OF REQUIRED CONVERTER RATING

Tables 14 and 15 show the line-current rms and line-to-line (within each loop/star) voltage-reference peaks, respectively. In accord with the plots from Figs. 8 and 9, it can be seen in these tables that the required converter current rating for $\lambda = 2$ does not surpass 180% (175.9% at worst) compared with $\lambda = 0$, and the necessary dc-link voltage is relatively similar for $\lambda = 2$ and $\lambda = 0$; on the other hand, for $\lambda = 1$ the dc-link voltage should be nearly doubled (increased to roughly 190%). It is worth pointing out that, even if the designer attempts to reduce converter current overrating by choosing $\lambda = 1$ instead of $\lambda = 2$ and increasing the dc-link voltage accordingly, the required line current rating may rise in more demanding fault scenarios (e.g., more than two OCLs), in general up to a maximum limit of 200% (currents of two adjacent phases with opposite electrical phase).

TABLE 14. Experimental Line-Current RMS (% of $i^{rc}/\sqrt{2}$) for $n = 12$.

$\lvert i_{\alpha\beta_1}\rvert$	$\lambda = 0$ SWC						$\lambda = 1$ SWC						$\lambda = 2$ SWC					
	$\mu = 1$	$\mu = 2$	$\mu = 3$	$\mu = 4$	$\mu = 5$	$\mu = 6$	$\mu = 1$	$\mu = 2$	$\mu = 3$	$\mu = 4$	$\mu = 5$	$\mu = 6$	$\mu = 1$	$\mu = 2$	$\mu = 3$	$\mu = 4$	$\mu = 5$	$\mu = 6$
78.0%	100.2	100.0	100.0	100.0	100.0	100.0	80.5	78.0	60.1	60.8	61.8	61.7	119.1	130.6	112.6	122.1	119.0	115.5
79.6%	–	100.0	100.0	100.0	100.0	100.0	82.0	79.5	61.4	62.0	62.9	62.9	121.5	130.7	114.9	124.6	121.5	117.8
80.6%	–	–	100.0	100.0	100.0	100.2	83.1	80.6	62.3	62.7	63.7	63.7	123.0	130.8	116.3	126.2	123.0	119.5
81.1%	–	–	100.0	100.0	100.3	–	83.6	81.1	62.5	63.2	64.2	64.1	123.8	130.8	117.1	126.9	123.7	120.1
81.5%	–	–	100.0	100.0	–	–	84.0	81.5	62.9	63.5	64.5	64.4	124.5	130.7	117.6	127.6	124.3	120.7
82.0%	–	–	–	100.0	–	–	84.5	82.0	63.2	63.9	64.8	64.8	125.2	131.3	118.4	128.4	125.2	121.4
84.0%	–	–	–	–	–	–	86.6	84.0	64.8	65.4	66.3	66.4	128.3	152.8	121.3	131.5	128.1	123.7
91.1%	–	–	–	–	–	–	93.9	91.0	70.2	70.9	71.9	71.9	154.0	–	131.5	144.4	154.1	139.9
91.9%	–	–	–	–	–	–	94.9	91.9	70.9	71.6	72.5	72.6	170.0	–	133.3	150.9	169.9	–
94.9%	–	–	–	–	–	–	101.4	94.9	73.1	73.9	74.9	75.0	–	–	147.0	175.9	–	–
95.3%	–	–	–	–	–	–	103.6	95.2	73.5	74.2	75.2	75.4	–	–	148.7	–	–	–
97.1%	–	–	–	–	–	–	118.4	97.5	74.9	76.0	78.7	78.7	–	–	–	–	–	–
98.7%	–	–	–	–	–	–	–	105.6	77.2	80.4	84.7	84.4	–	–	–	–	–	–
98.8%	–	–	–	–	–	–	–	106.2	77.4	80.8	85.0	–	–	–	–	–	–	–
98.9%	–	–	–	–	–	–	–	106.4	77.5	80.9	–	–	–	–	–	–	–	–

TABLE 15. Experimental Line-to-Line (Within a Loop or Star) Voltage-Reference Peak (in V) for $n = 12$.

$\lvert i_{\alpha\beta_1}\rvert$	$\lambda = 0$ SWC						$\lambda = 1$ SWC						$\lambda = 2$ SWC					
	$\mu = 1$	$\mu = 2$	$\mu = 3$	$\mu = 4$	$\mu = 5$	$\mu = 6$	$\mu = 1$	$\mu = 2$	$\mu = 3$	$\mu = 4$	$\mu = 5$	$\mu = 6$	$\mu = 1$	$\mu = 2$	$\mu = 3$	$\mu = 4$	$\mu = 5$	$\mu = 6$
78.0%	271	266	266	262	270	273	518	518	517	516	516	514	249	248	236	230	241	243
79.6%	–	265	266	263	271	276	516	516	516	517	516	515	249	248	237	227	239	243
80.6%	–	–	266	264	271	277	519	516	516	516	516	515	248	248	236	229	238	241
81.1%	–	–	265	263	271	–	517	515	517	515	515	515	248	250	235	228	238	241
81.5%	–	–	265	263	–	–	515	515	517	515	515	514	247	252	233	228	238	243
82.0%	–	–	–	263	–	–	515	515	517	515	514	514	247	251	232	227	237	242
84.0%	–	–	–	–	–	–	515	514	517	514	513	513	245	248	231	226	236	239
91.1%	–	–	–	–	–	–	511	511	514	509	510	510	236	–	229	222	226	249
91.9%	–	–	–	–	–	–	514	511	513	508	510	509	228	–	229	223	232	–
94.9%	–	–	–	–	–	–	513	509	511	507	508	507	–	–	224	224	–	–
95.3%	–	–	–	–	–	–	509	509	511	507	508	508	–	–	223	–	–	–
97.1%	–	–	–	–	–	–	511	510	509	506	506	506	–	–	–	–	–	–
98.7%	–	–	–	–	–	–	–	509	508	505	506	506	–	–	–	–	–	–
98.8%	–	–	–	–	–	–	–	508	508	505	506	–	–	–	–	–	–	–
98.9%	–	–	–	–	–	–	–	508	508	505	–	–	–	–	–	–	–	–

TABLE 16. Contactor States S1-S15 and Commands S4'-S5' During Transition Shown in Fig. 24 Using the Scheme From Fig. 11(e).

	S3	**S4**	**S4'**	**S5**	**S5'**	S7,S9,S12,S14	Other
$t < 0$ ms	**1**	**0**	**0**	**1**	**1**	0	1
0 ms $< t <$ 125 ms	**1**	**0**	**0**	**1**	**0**	0	1
125 ms $< t <$ 210 ms	**1**	**0**	**1**	**0**	**0**	0	1
210 ms $< t$	**1**	**1**	**1**	**0**	**0**	0	1

TABLE 17. Fault Phase-Current Constraints During Transition Shown in Fig. 24.

	Fault phase-current constraints
$t < 125$ ms	$i_a = i_c;\ i_c = i_e$
125 ms $< t <$ 210 ms	$i_a = i_c;\ i_c = i_e;\ i_d = i_f$
210 ms $< t$	$i_a = i_c;\ i_d = i_f$

5) TRANSITION FROM $\mu = 2$ TO $\mu = 3$ WITH $\lambda = 2$ SWC

Fig. 24 shows the current measurements during the proposed transition from $\mu = 2$ to $\mu = 3$, while $|i_{\alpha\beta_1}| = 80.0\%$ with OCLs in L1 and L3, using the type-A scheme from Section VI for $n = 12$ with $\lambda = 2$ [see Fig. 11(e)]. In this figure most of the signal labels are omitted, due to space constraints; nevertheless, the correspondence between colors and phase signals (top) is the same as in Figs. 21-23, and for the VSD signals (bottom) the colors are assigned in the same order as for the phases but following the order of the VSD axes according to (1). In addition, the contactor states/commands and the phase-current constraints during each stage of the transient are displayed in Tables 16 and 17, respectively.

Initially, L1' and L3' have zero line current, as L1 and L3, which are affected by OCLs. At $t = 0$ s the contactor S5, in series with L4', is commanded to open and the current references are modified so that the L4' line current is zero ($i_f \approx i_d$) as well. This contactor turns off at $t = 125$ ms, and then S4, between L3' and L4', is commanded to close. The latter occurs in effect at $t = 210$ ms. At that instant, the current references are changed so that current flow through L3' is exploited, working with $\mu = 3$ instead of $\mu = 2$, as intended.

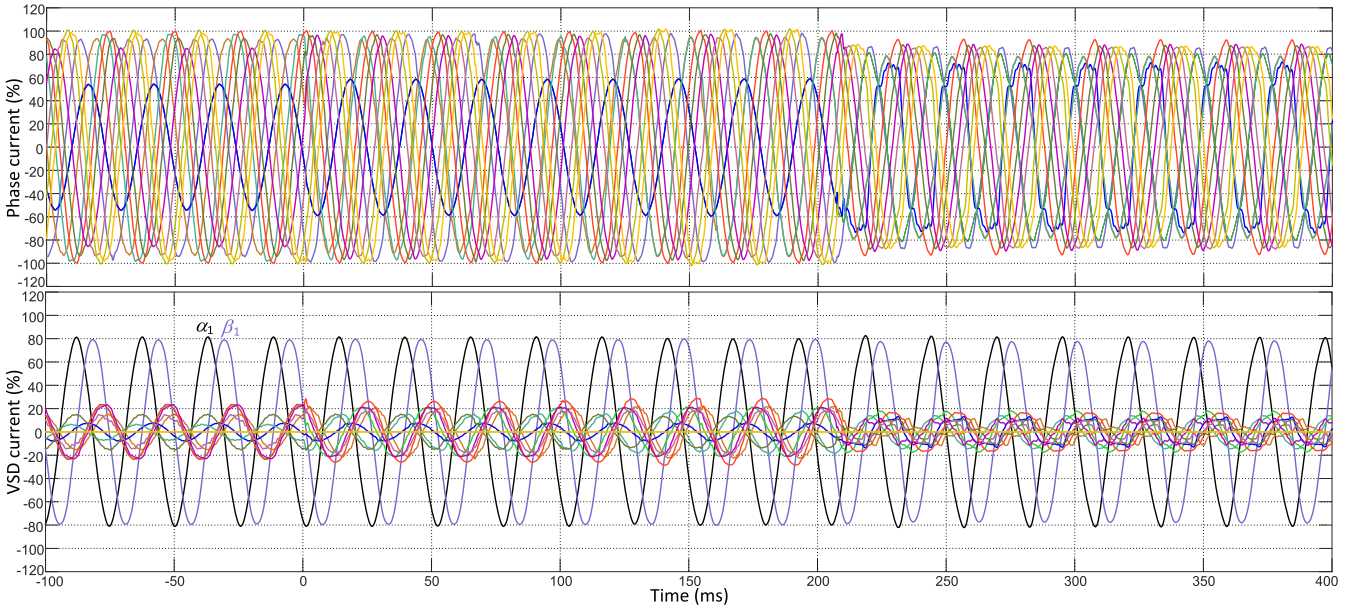

FIGURE 24. Experimental stator phase current during transition from $\mu = 2$ to $\mu = 3$, for $n = 12$ with $\lambda = 2$ SWC, OCLs in L1 and L3, and $|i_{\alpha\beta_1}| = 80.0\%$, by means of the method proposed in Section VI.

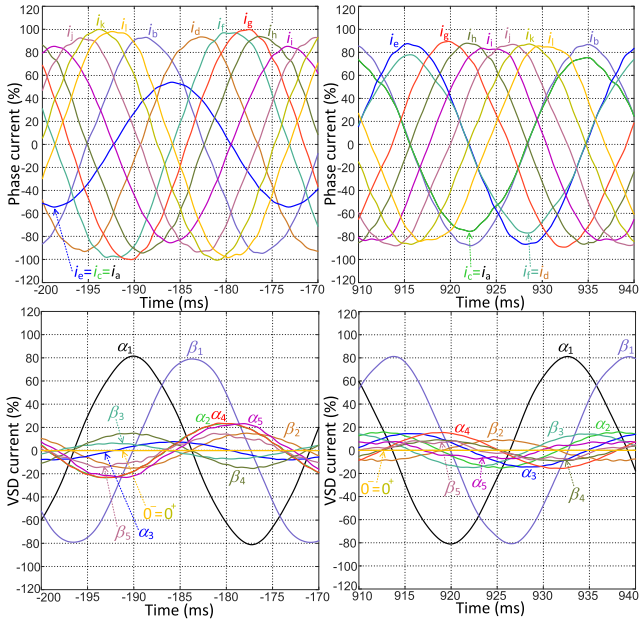

FIGURE 25. Experimental steady-state stator phase currents before and after transition shown in Fig. 24.

In Fig. 25, the steady-state waveforms before and after the transient (see the time values in the horizontal axis) are shown with more detail. The slight differences between the last cycles of Fig. 24 and the right part of Fig. 25 are due to the relatively slow dynamics of harmonic/imbalance current controllers (out of the scope of this paper), which take some time to be fully effective [58], [73]. Most importantly, it can be observed in Fig. 25 that, thanks to the proposed method, the maximum phase-current peaks are significantly decreased: from 100.0% (left) to 89.2% (right), thus allowing better potential MAT and SCL (also in agreement with the foregoing). In fact, without reducing the α_1-β_1 current amplitude (flux/torque), the total SCL is decreased from 100.9 W to 92.9 W.

VIII. CONCLUSION

In this paper, firstly, the performance of n-phase drives (n between 5 and 15) under two OCLs is addressed in terms of MAT (or equivalently, DF), SCL and required converter rating for various SWCs ($\lambda = 0, 1, 2$) suitable for symmetrical machines. Then, based on the conclusions of this study, a novel method is proposed to enhance significantly the postfault performance by adequately reconfiguring the connections between machine and converter without having to interrupt the drive operation. These contributions are explained with more details in the following.

The values of MAT, SCL and converter rating are determined and compared for multiple fault scenarios. In the first place, it is concluded that for two OCLs the $\lambda = 1$ SWC is also (as for single OCL) superior to the other SWCs in terms of SCL and MAT. In fact, it is shown that, for some conditions, the amount of enhancement is considerably larger than for one OCL. For instance, for $n = 6$ the improvement provided by $\lambda = 1$ can be up to a 28.9% of DF in comparison with $\lambda = 0$ for the same pair of OCLs, i.e., more than twice the increase (12.7%) of $\lambda = 1$ over $\lambda = 0$ shown in [8] for single OCL. Concerning the $\lambda = 2$ SWC, under two OCLs this SWC is still (as for one OCL) recommendable for $n > 10$, since then it provides SCL and MAT similar to $\lambda = 1$, but with more moderate converter voltage rating than $\lambda = 1$. In any case, to allow exploiting the potential MAT for two OCLs, the converter current rating should be increased further

than for single OCL, to a certain extent, either for $\lambda = 1$ or $\lambda = 2$. Nevertheless, this is an acceptable shortcoming when postfault performance is a priority.

Most importantly, based on this assessment of the performance for each scenario, a novel method is proposed to actively improve the postfault performance. Namely, electric schemes have been designed so that they can be inserted between a multiphase machine and converter, and when two OCLs occur, the connections between legs and stator terminals are deliberately modified in order to achieve significantly better SCL and MAT, without having to stop or disassemble the drive. For instance, for $n = 6$ with $\lambda = 1$, and for $n = 12$ with $\lambda = 2$, the DF can be raised in this manner in a quantity of 28.9% and 11.2%, respectively. These electric schemes are designed so that the number of extra devices needed is minimum. Furthermore, on the contrary to previous postfault reconfiguration techniques for multiphase drives such as that in [37], no accessible dc-link midpoint is required and no extra measures need to be added in order to avoid overcurrent and dc-link voltage oscillations. It should be remarked that this new reconfiguration strategy was also absent in [8], which only addressed (for the different SWCs) the case of single OCL, for which it would be of no interest (unlike for two OCLs) to alter the order of the converter-stator connections.

Experimental results with a six-phase induction motor and a twelve-phase permanent-magnet machine confirm the theoretical outcomes, as well as the functionality of the proposed method to dynamically alter the disposition of converter faulted/healthy legs.

The contributions presented here are particularly relevant for applications where high performance (regarding SCL and MAT) is expected to be desirable even under two OCLs, such as standalone or offshore wind generation and aircraft or military vehicles.

Potential subjects of future work include, e.g., a more accurate study of the dc-link voltage requirement taking into account the stator-impedance voltage drop for each specific fault and drive scenario, consideration of converter loss and different flux-derating/weakening approaches, extension to machines with asymmetrical winding arrangement, converters with more than n legs, etc.

REFERENCES

[1] E. Levi, "Multiphase electric machines for variable-speed applications," *IEEE Trans. Ind. Electron.*, vol. 55, no. 5, pp. 1893–1909, May 2008.

[2] E. Levi, R. Bojoi, F. Profumo, H. A. Toliyat, and S. Williamson, "Multiphase induction motor drives—A technology status review," *IET Electr. Power Appl.*, vol. 1, no. 4, pp. 489–516, Jul. 2007.

[3] E. Levi, F. Barrero, and M. J. Duran, "Multiphase machines and drives—Revisited," *IEEE Trans. Ind. Electron.*, vol. 63, no. 1, pp. 429–432, Jan. 2016.

[4] F. Barrero and M. J. Duran, "Recent advances in the design, modeling, and control of multiphase machines—Part I," *IEEE Trans. Ind. Electron.*, vol. 63, no. 1, pp. 449–458, Jan. 2016.

[5] M. Duran and F. Barrero, "Recent advances in the design, modeling and control of multiphase machines—Part 2," *IEEE Trans. Ind. Electron.*, vol. 63, no. 1, pp. 459–468, Jan. 2016.

[6] H. S. Che, M. J. Duran, E. Levi, M. Jones, W.-P. Hew, and N. A. Rahim, "Postfault operation of an asymmetrical six-phase induction machine with single and two isolated neutral points," *IEEE Trans. Power Electron.*, vol. 29, no. 10, pp. 5406–5416, Oct. 2014.

[7] W. N. W. A. Munim, M. Tousizadeh, and H. S. Che, "Effects of zero-sequence transformations and min-max injection on fault-tolerant symmetrical six-phase drives with single isolated neutral," *J. Power Electron.*, vol. 19, no. 4, pp. 968–979, Jul. 2019.

[8] A. G. Yepes, J. Doval-Gandoy, F. Baneira, and H. A. Toliyat, "Comparison of stator winding connections in multiphase drives under healthy operation and with one open converter leg," *IET Electr. Power Appl.*, vol. 14, no. 4, pp. 584–596, Apr. 2020.

[9] W. N. W. A. Munim, M. J. Duran, H. S. Che, M. Bermudez, I. Gonzalez-Prieto, and N. A. Rahim, "A unified analysis of the fault tolerance capability in six-phase induction motor drives," *IEEE Trans. Power Electron.*, vol. 32, no. 10, pp. 7824–7836, Oct. 2017.

[10] H. Xu, W. Huang, F. Bu, H. Liu, and X. Lin, "Control of five-phase dual stator-winding induction generator with an open phase," *IEEE Trans. Ind. Electron.*, vol. 66, no. 1, pp. 696–706, Jan. 2019.

[11] H. Liu, D. Wang, X. Yi, and F. Meng, "Torque ripple suppression under open-phase fault conditions in a five-phase induction motor with harmonic injection," *IEEE J. Emerg. Sel. Topics Power Electron.*, vol. 9, no. 1, pp. 274–288, Feb. 2021.

[12] A. S. Abdel-Khalik, A. S. Morsy, S. Ahmed, and A. M. Massoud, "Effect of stator winding connection on performance of five-phase induction machines," *IEEE Trans. Ind. Electron.*, vol. 61, no. 1, pp. 3–19, Jan. 2014.

[13] A. S. Abdel-Khalik, S. Ahmed, A. A. Elserougi, and A. M. Massoud, "Effect of stator winding connection of five-phase induction machines on torque ripples under open line condition," *IEEE/ASME Trans. Mechatronics*, vol. 20, no. 2, pp. 580–593, Apr. 2015.

[14] A. S. Abdel-Khalik, S. Ahmed, and A. M. Massoud, "Steady-state equivalent circuit of five-phase induction machines with different stator connections under open-line conditions," *IEEE Trans. Ind. Electron.*, vol. 63, no. 8, pp. 4651–4662, Aug. 2016.

[15] A. S. Abdel-Khalik, S. Ahmed, A. A. Elserougi, and A. M. Massoud, "A voltage-behind-reactance model of five-phase induction machines considering the effect of magnetic saturation," *IEEE Trans. Energy Convers.*, vol. 28, no. 3, pp. 576–592, Sep. 2013.

[16] H. M. Eldeeb, A. S. Abdel-Khalik, and C. M. Hackl, "Postfault full torque–speed exploitation of dual three-phase IPMSM drives," *IEEE Trans. Ind. Electron.*, vol. 66, no. 9, pp. 6746–6756, Sep. 2019.

[17] J. Sun, Z. Liu, Z. Zheng, and Y. Li, "An online global fault-tolerant control strategy for symmetrical multiphase machines with minimum losses in full torque production range," *IEEE Trans. Power Electron.*, vol. 35, no. 3, pp. 2819–2830, Mar. 2020.

[18] H. M. Eldeeb, A. S. Abdel-Khalik, J. Kullick, and C. M. Hackl, "Pre- and postfault current control of dual three-phase reluctance synchronous drives," *IEEE Trans. Ind. Electron.*, vol. 67, no. 5, pp. 3361–3373, May 2020.

[19] H. Guzman, M. J. Duran, F. Barrero, L. Zarri, B. Bogado, I. Gonzalez-Prieto, and M. R. Arahal, "Comparative study of predictive and resonant controllers in fault-tolerant five-phase induction motor drives," *IEEE Trans. Ind. Electron.*, vol. 63, no. 1, pp. 606–617, Jan. 2016.

[20] A. Tani, M. Mengoni, L. Zarri, G. Serra, and D. Casadei, "Control of multiphase induction motors with an odd number of phases under open-circuit phase faults," *IEEE Trans. Power Electron.*, vol. 27, no. 2, pp. 565–577, Feb. 2012.

[21] A. Mohammadpour, S. Sadeghi, and L. Parsa, "A generalized fault-tolerant control strategy for five-phase PM motor drives considering star, pentagon, and pentacle connections of stator windings," *IEEE Trans. Ind. Electron.*, vol. 61, no. 1, pp. 63–75, Jan. 2014.

[22] S. Jordan, C. D. Manolopoulos, and J. M. Apsley, "Winding configurations for five-phase synchronous generators with diode rectifiers," *IEEE Trans. Ind. Electron.*, vol. 63, no. 1, pp. 517–525, Jan. 2016.

[23] W. Cao, B. C. Mecrow, G. J. Atkinson, J. W. Bennett, and D. J. Atkinson, "Overview of electric motor technologies used for more electric aircraft (MEA)," *IEEE Trans. Ind. Electron.*, vol. 59, no. 9, pp. 3523–3531, Sep. 2012.

[24] M. J. Duran, I. Gonzalez-Prieto, N. Rios-Garcia, and F. Barrero, "A simple, fast, and robust open-phase fault detection technique for six-phase induction motor drives," *IEEE Trans. Power Electron.*, vol. 33, no. 1, pp. 547–557, Jan. 2018.

[25] F. Baneira, J. Doval-Gandoy, A. G. Yepes, O. Lopez, and D. Perez-Estevez, "Control strategy for multiphase drives with minimum losses in the full torque operation range under single open-phase fault," *IEEE Trans. Power Electron.*, vol. 32, no. 8, pp. 6275–6285, Aug. 2017.

[26] A. G. Yepes, J. Doval-Gandoy, F. Baneira, and H. A. Toliyat, "Control strategy for dual three-phase machines with two open phases providing minimum loss in the full torque operation range," *IEEE Trans. Power Electron.*, vol. 33, no. 12, pp. 10044–10050, Dec. 2018.

[27] F. Baneira, J. Doval-Gandoy, A. G. Yepes, O. Lopez, and D. Perez-Estevez, "Comparison of postfault strategies for current reference generation for dual three-phase machines in terms of converter losses," *IEEE Trans. Power Electron.*, vol. 32, no. 11, pp. 8243–8246, Nov. 2017.

[28] G. Sala, M. Mengoni, G. Rizzoli, M. Degano, L. Zarri, and A. Tani, "Impact of star connection layouts on the control of multiphase induction motor drives under open-phase fault," *IEEE Trans. Power Electron.*, vol. 36, no. 4, pp. 3717–3726, Apr. 2021.

[29] M. Salehifar, R. S. Arashloo, J. M. Moreno-Equilaz, V. Sala, and L. Romeral, "Fault detection and fault tolerant operation of a five phase PM motor drive using adaptive model identification approach," *IEEE J. Emerg. Sel. Topics Power Electron.*, vol. 2, no. 2, pp. 212–223, Jun. 2014.

[30] N. Bianchi, S. Bolognani, and M. D. Pre, "Strategies for the fault-tolerant current control of a five-phase permanent-magnet motor," *IEEE Trans. Ind. Appl.*, vol. 43, no. 4, pp. 960–970, Jul. 2007.

[31] R. S. Arashloo, J. L. R. Martinez, M. Salehifar, and M. Moreno-Eguilaz, "Genetic algorithm-based output power optimisation of fault tolerant five-phase brushless direct current drives applicable for electrical and hybrid electrical vehicles," *IET Electr. Power Appl.*, vol. 8, no. 7, pp. 267–277, Aug. 2014.

[32] H.-M. Ryu, J.-W. Kim, and S.-K. Sul, "Synchronous-frame current control of multiphase synchronous motor under asymmetric fault condition due to open phases," *IEEE Trans. Ind. Appl.*, vol. 42, no. 4, pp. 1062–1070, Jul. 2006.

[33] M. Tousizadeh, H. S. Che, A. S. Abdel-Khalik, W. N. W. A. Munim, J. Selvaraj, and N. A. Rahim, "Effects of flux derating methods on torque production of fault-tolerant polyphase inductiondrives," *IET Electr. Power Appl.*, vol. 15, no. 5, pp. 616–628, May 2021.

[34] I. Gonzalez-Prieto, M. J. Duran, N. Rios-Garcia, F. Barrero, and C. Martin, "Open-switch fault detection in five-phase induction motor drives using model predictive control," *IEEE Trans. Ind. Electron.*, vol. 65, no. 4, pp. 3045–3055, Apr. 2018.

[35] P. Garcia-Entrambasaguas, I. González-Prieto, and M. J. Duran, "Single-index open-phase fault detection method for six-phase electric drives," *IEEE Trans. Ind. Electron.*, vol. 67, no. 12, pp. 10233–10242, Dec. 2020.

[36] J. M. Apsley, "Derating of multiphase induction machines due to supply imbalance," *IEEE Trans. Ind. Appl.*, vol. 46, no. 2, pp. 798–805, Mar./Apr. 2010.

[37] A. G. Yepes, J. Doval-Gandoy, and H. A. Toliyat, "Strategy with smooth transitions and improved Torque–Speed region and stator copper loss for two-level asymmetrical six-phase induction motor drives under switch faults," *IEEE Trans. Power Electron.*, vol. 36, no. 2, pp. 1954–1969, Feb. 2021.

[38] B. Chikondra, U. R. Muduli, and R. K. Behera, "An improved open-phase fault-tolerant DTC technique for five-phase induction motor drive based on virtual vectors assessment," *IEEE Trans. Ind. Electron.*, vol. 68, no. 6, pp. 4598–4609, Jun. 2021.

[39] Y. Geng, Z. Lai, Y. Li, D. Wang, R. Chen, and P. Zheng, "Sensorless fault-tolerant control strategy of six-phase induction machine based on harmonic suppression and sliding mode observer," *IEEE Access*, vol. 7, pp. 110086–110102, 2019.

[40] Y. Zhou, X. Lin, and M. Cheng, "A fault-tolerant direct torque control for six-phase permanent magnet synchronous motor with arbitrary two opened phases based on modified variables," *IEEE Trans. Energy Convers.*, vol. 31, no. 2, pp. 549–556, Jun. 2016.

[41] M. J. Duran, I. Gonzalez-Prieto, M. Bermudez, F. Barrero, H. Guzman, and M. R. Arahal, "Optimal fault-tolerant control of six-phase induction motor drives with parallel converters," *IEEE Trans. Ind. Electron.*, vol. 63, no. 1, pp. 629–640, Jan. 2016.

[42] A. Shawier, A. S. Abdel-Khalik, R. A. Hamdy, K. H. Ahmed, and S. Ahmed, "Postfault operation of five-phase induction machine with minimum total losses under single open-phase fault," *IEEE Access*, vol. 8, pp. 208696–208706, 2020.

[43] S. Ouenzerfi, H. Zahr, M. Trabelsi, E. Semail, S. Harmand, and R. Boubaker, "3-D multi-nodal thermal modelling for fault-tolerant machine," in *Proc. IEEE Int. Conf. Ind. Technol. (ICIT)*, Feb. 2019, pp. 1551–1556.

[44] A. Boglietti, I. R. Bojoi, S. Rubino, and M. Cossale, "Overload capability of multiphase machines under normal and open-phase fault conditions: A thermal analysis approach," *IEEE Trans. Ind. Appl.*, vol. 56, no. 3, pp. 2560–2569, May 2020.

[45] H. Zhang, P. Giangrande, G. Sala, Z. Xu, W. Hua, V. Madonna, D. Gerada, and C. Gerada, "Thermal model approach to multisector three-phase electrical machines," *IEEE Trans. Ind. Electron.*, vol. 68, no. 4, pp. 2919–2930, Apr. 2021.

[46] Z. Liang, D. Liang, P. Kou, and S. Jia, "Postfault control and harmonic current suppression for a symmetrical dual three-phase SPMSM drive under single-phase open-circuit fault," *IEEE Access*, vol. 8, pp. 67674–67686, 2020.

[47] B. A. Welchko, T. A. Lipo, T. M. Jahns, and S. E. Schulz, "Fault tolerant three-phase AC motor drive topologies: A comparison of features, cost, and limitations," *IEEE Trans. Power Electron.*, vol. 19, no. 4, pp. 1108–1116, Jul. 2004.

[48] W. Zhang, D. Xu, P. N. Enjeti, H. Li, J. T. Hawke, and H. S. Krishnamoorthy, "Survey on fault-tolerant techniques for power electronic converters," *IEEE Trans. Power Electron.*, vol. 29, no. 12, pp. 6319–6331, Dec. 2014.

[49] A. Li, D. Jiang, Z. Liu, X. Sun, and W. Kong, "Unified analysis of winding connection sequence in series-end winding topology," *IEEE Trans. Ind. Appl.*, vol. 57, no. 1, pp. 516–527, Jan. 2021.

[50] D. Dujic, M. Jones, and E. Levi, "Analysis of output current-ripple RMS in multiphase drives using polygon approach," *IEEE Trans. Power Electron.*, vol. 25, no. 7, pp. 1838–1849, Jul. 2010.

[51] N. K. Nguyen, E. Semail, F. Meinguet, P. Sandulescu, X. Kestelyn, and B. Aslan, "Different virtual stator winding configurations of open-end winding five-phase PM machines for wide speed range without flux weakening operation," in *Proc. 15th Eur. Conf. Power Electron. Appl. (EPE)*, Sep. 2013, pp. 1–8.

[52] J. S. Edelson, "High phase order motor with mesh connected windings," U.S. Patent 6 831 430, Dec. 14, 2004.

[53] A. Sayed-Ahmed and N. A. O. Demerdash, "Fault-tolerant operation of delta-connected scalar- and vector-controlled AC motor drives," *IEEE Trans. Power Electron.*, vol. 27, no. 6, pp. 3041–3049, Jun. 2012.

[54] A. G. Yepes and J. Doval-Gandoy, "Performance evaluation and improvement of symmetrical six-phase drives under two open legs with star and hexagon connections," in *Proc. IEEE Energy Convers. Congr. Exposit. (ECCE)*, Oct. 2020, pp. 5328–5335.

[55] G. Joksimovic, M. Mezzarobba, A. Tessarolo, and E. Levi, "Optimal selection of rotor bar number in multiphase cage induction motors," *IEEE Access*, vol. 8, pp. 135558–135568, 2020.

[56] D. M. Ionel, M. Popescu, S. J. Dellinger, T. J. E. Miller, R. J. Heideman, and M. I. McGilp, "On the variation with flux and frequency of the core loss coefficients in electrical machines," *IEEE Trans. Ind. Appl.*, vol. 42, no. 3, pp. 658–667, May 2006.

[57] E. Levi, D. Dujic, M. Jones, and G. Grandi, "Analytical determination of DC-bus utilization limits in multiphase VSI supplied AC drives," *IEEE Trans. Energy Convers.*, vol. 23, no. 2, pp. 433–443, Jun. 2008.

[58] A. G. Yepes, J. Doval-Gandoy, and H. A. Toliyat, "Multifrequency current control for n-phase machines including antiwindup and distortion-free saturation with full dc-bus utilization," *IEEE Trans. Power Electron.*, vol. 34, no. 10, pp. 9891–9905, Oct. 2019.

[59] K. Hu, Z. Liu, Y. Yang, F. Iannuzzo, and F. Blaabjerg, "Ensuring a reliable operation of two-level IGBT-based power converters: A review of monitoring and fault-tolerant approaches," *IEEE Access*, vol. 8, pp. 89988–90022, 2020.

[60] A. Tessarolo, F. Luise, S. Pieri, A. Benedetti, M. Bortolozzi, and M. De Martin, "Design for manufacturability of an off-shore direct-drive wind generator: An insight into additional loss prediction and mitigation," *IEEE Trans. Ind. Appl.*, vol. 53, no. 5, pp. 4831–4842, Sep. 2017.

[61] P. Garg, S. Essakiappan, H. S. Krishnamoorthy, and P. N. Enjeti, "A fault-tolerant three-phase adjustable speed drive topology with active common-mode voltage suppression," *IEEE Trans. Power Electron.*, vol. 30, no. 5, pp. 2828–2839, May 2015.

[62] N. Bianchi, S. Bolognani, M. Zigliotto, and M. Zordan, "Innovative remedial strategies for inverter faults in IPM synchronous motor drives," *IEEE Trans. Energy Convers.*, vol. 18, no. 2, pp. 306–314, Jun. 2003.

[63] A. Birolini, *Reliability Engineering: Theory and Practice*. New York, NY, USA: Springer, 2010.
[64] T. J. dos Santos Moraes, E. Semail, N. K. Nguyen, F. Meinguet, and M. Guerin, "New electrical inversed-series connection for even-phase symmetrical PMSMs," *IEEE Trans. Power Electron.*, vol. 33, no. 9, pp. 7938–7947, Sep. 2018.
[65] M. Slunjski, O. Dordevic, M. Jones, and E. Levi, "Symmetrical/asymmetrical winding reconfiguration in multiphase machines," *IEEE Access*, vol. 8, pp. 12835–12844, 2020.
[66] I. Subotic, N. Bodo, E. Levi, M. Jones, and V. Levi, "Isolated chargers for EVs incorporating six-phase machines," *IEEE Trans. Ind. Electron.*, vol. 63, no. 1, pp. 653–664, Jan. 2016.
[67] M. S. Diab, A. A. Elserougi, A. S. Abdel-Khalik, A. M. Massoud, and S. Ahmed, "A nine-switch-converter-based integrated motor drive and battery charger system for EVs using symmetrical six-phase machines," *IEEE Trans. Ind. Electron.*, vol. 63, no. 9, pp. 5326–5335, Sep. 2016.
[68] M. Y. Metwly, M. S. Abdel-Majeed, A. S. Abdel-Khalik, R. A. Hamdy, M. S. Hamad, and S. Ahmed, "A review of integrated on-board ev battery chargers: Advanced topologies, recent developments and optimal selection of FSCW slot/pole combination," *IEEE Access*, vol. 8, pp. 85216–85242, 2020.
[69] A. Elserougi, M. S. Diab, A. Massoud, and S. Ahmed, "A six-arm symmetrical six-phase hybrid modular multilevel converter with unidirectional current full-bridge submodules," *IEEE J. Emerg. Sel. Topics Power Electron.*, early access, Jun. 8, 2020, doi: 10.1109/JESTPE.2020.3000654.
[70] G. Rezazadeh, F. Tahami, G.-A. Capolino, S. Vaschetto, Z. Nasiri-Gheidari, and H. Henao, "Improvement of concentrated winding layouts for six-phase squirrel cage induction motors," *IEEE Trans. Energy Convers.*, vol. 35, no. 4, pp. 1727–1735, Dec. 2020.
[71] A. S. Abdel-Khalik, M. S. Abdel-Majeed, and S. Ahmed, "Effect of winding configuration on six-phase induction machine parameters and performance," *IEEE Access*, vol. 8, pp. 223009–223020, 2020.
[72] L. Shao, W. Hua, J. Soulard, Z.-Q. Zhu, Z. Wu, and M. Cheng, "Electromagnetic performance comparison between 12-phase switched flux and surface-mounted PM machines for direct-drive wind power generation," *IEEE Trans. Ind. Appl.*, vol. 56, no. 2, pp. 1408–1422, Mar. 2020.
[73] H. S. Che, E. Levi, M. Jones, W.-P. Hew, and N. A. Rahim, "Current control methods for an asymmetrical six-phase induction motor drive," *IEEE Trans. Power Electron.*, vol. 29, no. 1, pp. 407–417, Jan. 2014.
[74] S. N. Vukosavic, L. S. Peric, and E. Levi, "AC current controller with error-free feedback acquisition system," *IEEE Trans. Energy Convers.*, vol. 31, no. 1, pp. 381–391, Mar. 2016.
[75] S. N. Vukosavic, L. S. Peric, and E. Levi, "Digital current controller with error-free feedback acquisition and active resistance," *IEEE Trans. Ind. Electron.*, vol. 65, no. 3, pp. 1980–1990, Mar. 2018.

ALEJANDRO G. YEPES (Senior Member, IEEE) received the M.Sc. and Ph.D. degrees in electrical engineering from the Universidade de Vigo, Vigo, Spain, in 2009 and 2011, respectively.

Since 2008, he has been working with the Applied Power Electronics Technology Research Group, Universidade de Vigo. From August 2016 to June 2018, he was with the Department of Electrical and Computer Engineering, Texas A&M University, College Station, TX, USA, after which he returned to the Universidade de Vigo. His research interest includes ac power conversion, with special focus, currently, on multiphase drives.

JESÚS DOVAL-GANDOY (Member, IEEE) received the M.Sc. degree in electrical engineering from the Polytechnic University of Madrid, Madrid, Spain, in 1991, and the Ph.D. degree in electrical engineering from the Universidade de Vigo, Vigo, Spain, in 1999. He is currently a Professor and the Head of the Applied Power Electronics Technology Research Group (APET), Universidade de Vigo.

His research interest includes ac power conversion.